TECHNISCHE UNIVERSITÄT WIEN
Vienna University of Technology

D I P L O M A R B E I T

CHARACTERIZATION OF PROTEIN-PROTEIN INTERACTIONS AT THE CELL MEMBRANE USING NANOPATTERNED SURFACES

Ausgeführt am Institut für Angewandte Physik

der Technischen Universität Wien

unter der Anleitung von

Univ.Prof. Dipl.-Ing. Dr.techn. Gerhard Schütz

durch

Martin Fölser

Großambergstraße 79

4048 Puchenau

Wien, am 16.12.2014

ABSTRACT

Protein-protein interaction in live cell membranes can be shown by labelling the proteins of interest and mapping the distribution of the respective fluorescent signal in the membrane. The difficulties of analyzing colocalization experiments can be circumvented by arranging one of the proteins as bait in a well-defined pattern in the cell membrane and measuring and comparing the abundance and diffusion characteristics of the second protein in bait-rich and bait-depleted areas. To create those patterns the bait protein is immobilized by antibodies that are linked to Streptavidin, which is deposited in an underlying structure using soft lithography. The standard protocols for this technique allow only the creation of feature sizes which are at least one order of magnitude larger than the supposed size of functional domains in the cell membrane. To miniaturize the size of patterns to widths of 200 nm and below great efforts in lithography are required as substrates have to be chosen more carefully and novel stamp materials have to be used. In my diploma thesis I studied and characterized nanopatterns generated by novel POSS materials using advanced microscopy technique such as TIRF, single molecule superresolution microscopy and AFM. Finally, I applied the system for preliminary experiments on live cells.

KURZZUSAMMMENFASSUNG

Die Wechselwirkungen zwischen Proteinen kann in der Membran lebender Zellen dadurch gemessen werde, dass diese mit fluoreszierenden Proteinen oder Farbstoffen markiert und abgebildet werden. Da bei der Auswertung des Überlapps der gemessenen Signale mannigfaltige Probleme auftreten, wurde von unserer Gruppe vorgeschlagen, ein Protein in einem vorgegbenen Muster anzuordnen und das Vorkommen sowie das Diffusionsverhalten des Zweiten mit dem Muster des Ersten zu vergleichen. Die Erstellung dieser Muster erfolgt durch eine Bindung über Antikörper an eine unterliegende Struktur aus Streptavidin, die mittels Mikrokontakt-Stempeldruck hergestellt wurde. Technisch waren die Standardverfahren hierzu nur in der Lage, Strukturen zu generieren, die eine Größenordnung über den vermuteten funktionellen Bereichen in der Zellmembran liegen. Zur Miniaturisierung auf Größen von 200 nm und darunter ist es nötig neue Materialien zu verwenden und Protokolle zu optimieren. In meiner Diplomarbeit studierte und charakterisierte ich Nanostrukturen, welche über POSS Materialien erzeugt wurden, mittels moderner Mikroskopietechniken wie z.B. TIRF Mikroskopie, hochaufgelöste Einzelmolekül Mikroskopie, sowie AFM. Schließlich führte ich präliminäre Experimente an lebenden Zellen durch.

CONTENTS

1 INTRODUCTION/MOTIVATION

1.1 IMMUNOLOGICAL BACKGROUND

The immune system can be separated into two subclasses. The innate immune system is found in nearly all forms of life. It provides a palette of tools to generically recognize components that could potentially be harmful to the organism and to attack those pathogens. The response of this system is fast but not all pathogens can be fought by it.

The adaptive immune system, which is only found in vertebrates, allows for stronger immune responses by specifically focusing on a single kind of pathogen. These pathogens include bacteria, viruses, microorganisms, pollen and also transplanted tissue and transfused blood cells. Their surfaces exhibit a characteristic set of proteins and polysaccharides that can be recognized by antibodies. These molecules or parts of molecules are called antigens. Professional antigen presenting cells, most notably dendritic cells, are in the vanguard of the adaptive immune system. They incorporate the pathogens at the site of infection, migrate through the lymphatic system to the lymph nodes and present the obtained antigen on their surface so that naïve T-cells can probe them. If T-cells recognize an antigen, they get activated, proliferate and differentiate into natural killer T-cells (which can attack cells), T helper cells (releases cytokines that activates other immune cells, e.g. it stimulates B-cells to produce antibodies) and other subtypes that aid and regulate the immune response. Information on the antigen gets stored in memory cells that persist in the organism for a long time and quickly proliferate on repeated contact with the pathogen.

The focus of our group lies on the biophysical characterization of the immunological synapse, the contact between the antigen presenting cell and the T-cell (Figure 1, left). A T-cell specifically recognizes one single antigen. As there is a plethora of possibilities how an antigen might look like, only a small number of T-cells in the organism that are activated upon contact with a given antigen is available to trigger an immune response. This demands two requirements which do not comply. On the one hand the mechanism has to be sensitive, so that no vital information on an attacking pathogen gets lost. On the other hand only perfectly matching T-cells should be activated to provide an efficient immune response and to suppress false alarms.

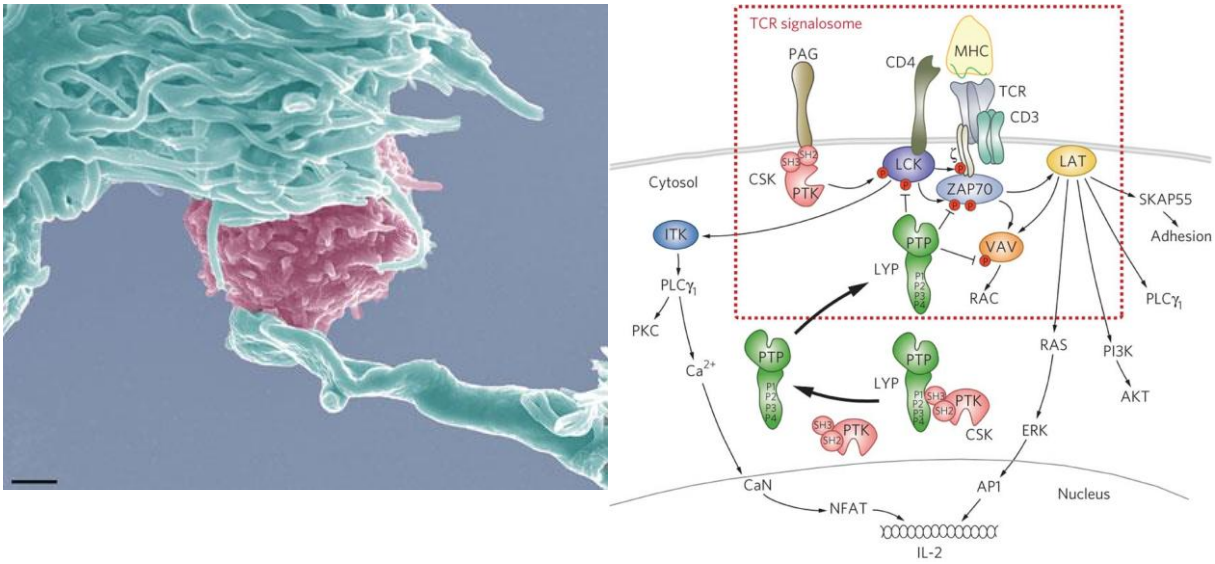

FIGURE 1: LEFT: ELECTRON MICROSCOPY IMAGE OF DENDRITIC CELL SENSING LYMPHOCYTE (SCHWARTZ, 2004); RIGHT: KEY PROTEINS IN THE TCR-SIGNALING PATHWAY, (VANG ET AL., 2012)

A large number of molecules take part in the activation pathway (Figure 1, right). From the APC side this is most notably the major histocompatibility complex class II (MHCII) that presents the antigen. Its counterpart on the T cell is the T-cell receptor (TCR). Co-receptors provide stability of the contact or fulfill co-stimulatory roles. One of them is CD4, a glycoprotein that recruits the tyrosine kinase Lck to the TCR to amplify its signal and to activate the signaling cascade which leads to Ca^{++}-flux in the cytosol and culminates in T-cell proliferation and differentiation.

1.2 GOING NANO

The interaction of CD4 and Lck has been measured by our group using the micropatterning technique by forcing CD4 in well-defined areas and measuring the abundance of Lck in these areas (Schwarzenbacher et al., 2008). The domains contributing to the affinity could be identified.

The spatial distribution of either protein in the immunological synapse could not be addressed as the size of CD4 enriched regions had a diameter of 3 µm, which is at least one order of magnitude larger than the presumed size of functional domains in the synapse. The Nyquist-Shannon sampling theorem states that in order to resolve features sampling intervals of half the resolution are needed. So in order to distinguish features placed 100 nm apart, measurement points with a periodicity of 50 nm are needed. While such features can be resolved by optical superresolution microscopy, the experimental platform to facilitate the enrichment of proteins has not been available. The scope of this thesis was to test the conditions under which patterns with a feature size of 230 nm can be fabricated in order to use this knowledge to produce pattern with even higher feature frequency.

2 BACKGROUND

2.1 FLUORESCENCE MICROSCOPY

Traditional light microscopy methods probe the optical properties of the sample (absorption and refraction) providing just enough contrast to distinguish certain cell organelles. As a consequence since the beginning of modern biochemistry in the 1930s modifications of the sample were made. Dyes with high affinities for specific organelles were discovered which allow deliberate staining of those cell elements. A further improvement was the usage of molecules that would reemit light upon illumination. The development of higher quantum yields of those dyes, more variants of linking those to molecules of interest and specialized applications accelerated the triumph of fluorescence microscopy (FM) in molecular biology.

Fluorescence was termed by Stokes, its detailed description can be given within quantum mechanics. The simplest model consists of a molecule with ground state S_0 and first excited state S_1. The atom can be excited to the higher electronic state by absorption of light with photon energy $h\nu_{ex}$ where h is Planck's constant and ν is the frequency of the light:

$$S_0 + h\nu_{ex} \rightarrow S_1$$

The molecule can either relax to its ground state by losing its excess energy through a non-radiative channel or by emitting a fluorescent photon with energy $h\nu_{em}$ a few nanoseconds after the absorption process:

$$S_1 \rightarrow S_0 + h\nu_{em} + E_{heat}$$

The Jablonski diagram (Figure 9), which visualizes this system can be seen in section 2.5.4 where the photochemistry involved in superresolution microscopy is discussed in more detail. Here, E_{heat} is energy loss through dissipative processes; energy conservation states that thus the energy of the incident photon is larger than the energy of the emitted photon:

$$h\nu_{ex} > h\nu_{em}$$

In the wavelength picture ($\lambda = \frac{c}{\nu}$, where c is the speed of light) this means that the emitted light λ_{em} is red-shifted compared to the absorbed light λ_{ex}:

$$\lambda_{ex} < \lambda_{em}$$

The difference between the band maxima of the absorption and emission spectra is called Stokes shift and is caused by vibrational relaxation and collision processes. The effect can be accounted in the model system by adding vibrational states. The energy states and consequently the fluorescent wavelength are characteristic for the molecule and can be used to identify the molecule, however larger molecules like the markers used for fluorescence

microscopy exhibit manifold rotational and vibrational degrees of freedom broadening the spectra. At least discerning three different labels in the visible range is easily possible with a reasonable choice of fluorescent molecules. The Stokes shift is a critical property for FM as it allows exciting a fluorophore with monochromatic light and detection in another band of the visible spectrum. Using a well-chosen set of filters the signal of the emitted light can be recorded without spectral overlap with the high intensity excitation illumination, which would otherwise cover the relatively low fluorescent signal.

Fluorophores used in FM commonly have structures containing aromatic rings with double bonds that easily distribute outer valence electrons over a large area, as they have excellent absorption efficiency, require low excitation intensities and exhibit large Stoke shifts. (Sauer, Hofkens, & Enderlein, 2011). The excitation spectrum of fluorophores represents the available energy levels of the molecule; the probability of an absorption event if light travels through a fluorophore containing solution is called molar extinction coefficient, ϵ, in units of $M^{-1}cm^{-1}$. Organic fluorophores have extinction coefficients up to $250{,}000\ M^{-1}cm^{-1}$ (Berlier et al., 2003), fluorescent proteins up to $150{,}000\ M^{-1}cm^{-1}$ (Shaner et al., 2013). The brightness of the fluorophore is the product of molar extinction coefficient and quantum yield. Quantum yield is the ratio of fluorescence emission to non-radiative energy losses. Recently fluorophores that probe their molecular environment have become of increasing importance. Their optical properties alter on e.g. binding to calcium or a change of acidity or transmembrane potential (Kuhn, Fromherz, & Denk, 2004).

One of the strengths of fluorescence microscopy is the ability to label specific kinds of proteins. A common strategy is to genetically encode fluorescent proteins (FP) in the genome of the cell. The experiments are conducted in such a way that at expression the FP is attached to the protein of interest. So the fluorescence signal of the FP marks the position of its partner. Care has to be taken, that the co-expression does not impede the protein's functionality. Due to the intrinsic linking of FP and protein the method can be used also for labeling intracellular proteins. The lack of excessive unbound dye minimizes background fluorescence.

The first FP, the green fluorescent protein (GFP) was originally found in Aequorea jellyfish. GFP has a typical barrel structure formed of beta sheets; in its core resides the chromophore – a Ser-Tyr-Gly peptide, which is modified due to interaction with inward facing side chains of the barrel to 4-(p-hydroxybenzylidene)imidazolidin-5-one (Shimomura, 1979). In the meantime various mutations of GFP and FPs from other animals have been found. They have been screened not only for better brightness and photostability characteristics, but also a low tendency to oligomerize is desired.

Organic dyes, small organic fluorophores such as rhodamine and cyanine derivates, usually are brighter compared to FPs and outperform them in terms of photostability. The extrinsic

labelling process however requires ligands connecting the fluorophore to the molecule of interest, which can set constraints to their application. A large number of substances that bind to certain proteins is known. Also specific antibodies can be utilized to label the protein of interest. Fluorophores can be conjugated to those substances and antibodies and allow labelling. The disadvantage is the rather low labelling efficiency and that only proteins in the outer regions of the plasma membrane are targetable unless the cells are permeabilized. Furthermore, the location of the fluorophore is not necessarily the position of the protein of interest. Due to the size of the antibody markers are slightly dislocated from the actual site of the protein of interest adding 10-20 nm to the localization uncertainty (Patterson, Davidson, Manley, & Lippincott-Schwartz, 2010). On the plus side the number of photons emitted from organic fluorophores is up to one order of magnitude higher than from FP. Quantum dots might be mentioned in this context as their labelling approach is similar, the application in life sciences of those semiconductor nanocrystals is however limited by their challenging passivating and targeting chemistry and by their comparably large size (Jaiswal & Simon, 2004).

2.2 THE MICROSCOPY SETUP

Two different microscope setups were used, in the following referred to as SDT 2 and SDT 4. Both are based on Zeiss Axiovert 200 inverted microscopes with home-built laser light sources on vibration reducing optical tables. Each setup has a 405 nm (near-UV) laser for fluorophore activation (SDT 2: Coherent Innova 90c; SDT 4: Crystalaser) and three lasers for imaging in the 488 nm (blue) channel (SDT 2 & SDT 4: Toptica iBeam smart 200mW), the 532 nm (green) channel (SDT 2 and SDT 4 shared: Spectra physics Millenia 6s) and the 647 nm (red) channel (both SDT 2 and SDT 4: Toptica iBeam smart 200mW). The Toptica lasers can be directly modulated, green light can be switched with an acousto-optic modulator, near-UV illumination requires a manually triggered mechanical shutter.

To improve the beam shape a spatial filter is inserted in the imaging beam lines of SDT 2. It consists of two lenses and a pinhole, whereby the pinhole is placed in the focal point of the first lens. So in the plane of the pinhole the Fourier-transform of the incoming beam's transverse intensity distribution can be seen. Shifting the pinhole allows the selective transmission of the desired orders, which for even illumination is the lowest mode TEM_{00}. The second lens transforms the beam back to its parallel form. The two lenses also act as a telescope: the beam width after the telescope is magnified proportional to the ratio of the focal lengths of the second and first lens.

All four beams on both setups are overlaid with the use of dichroic mirrors and coupled into a telescope (Figure 2). On SDT 4 this telescope is the only way to change the diameter of the beam; adjusting single colors independently is not possible. The primary use of the telescope

on SDT 2 is to focus the beam in the back focal plane of the objective. On SDT 4 this is accomplished by a special illumination unit in the microscope.

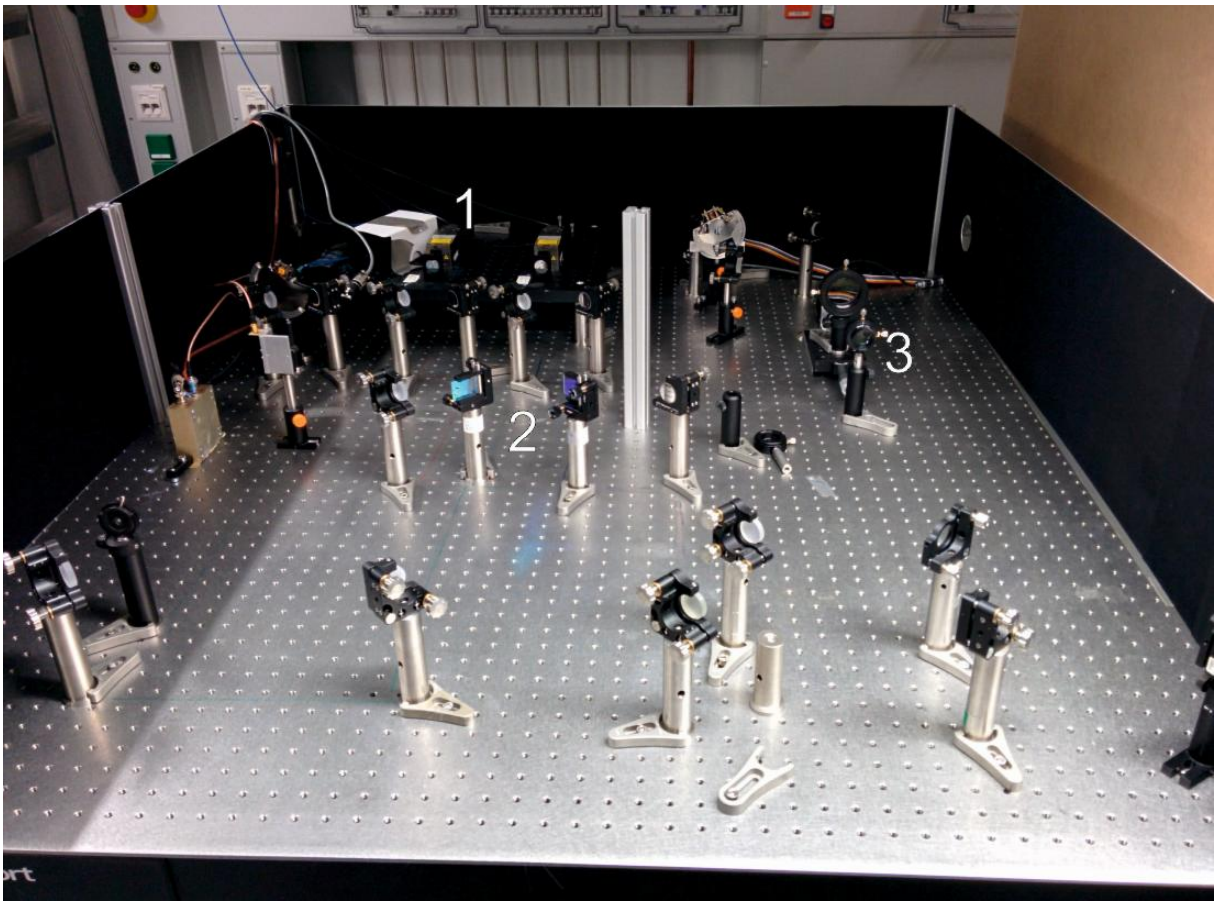

FIGURE 2: MULTI-COLOR LASER BEAM OVERLAY ON SDT 4. THE LASER SOURCES (1) ARE EITHER COMPACT DIODE LASERS MOUNTED ON THE TABLE OR OPTICAL FIBERS THAT TRANSMIT LIGHT CREATED BY A TI:SAPPHIRE LASER IN THE NEIGHBORING ROOM. THE BEAMS ARE OVERLAYED USING DICHROIC MIRRORS (2). SIZE AND DIVERGENCE OF THE BEAM CAN BE ADJUSTED WITH A TELESCOPE (3).

A periscope couples the beam into the rear port of the Zeiss microscope. To shift the lateral position of the beam on the back focal plane of the objective the lower mirror is mounted on a motorized moveable table on SDT 2; the upper mirror can be tilted using a motorized screw an SDT 4.

Illumination and detection of the fluorescence signal happen on the same side – on the bottom side at inverted microscopes. This arrangement is termed epifluorescence illumination. One of the crucial factors as far as both illumination and imaging are concerned is thus the objective. For this thesis two 100x oil immersion objectives were in use: a Zeiss alpha Plan-Apochromat (NA =1.46) and a Olympus PlanApo (NA=1.45).

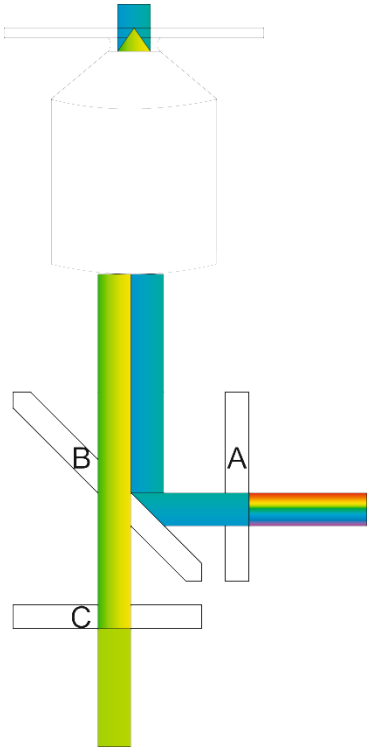

FIGURE 3: WORKING PRINCIPLE OF EPI-FLUORESCENCE MICROSCOPES. THE EXCITATION FILTER (A) ONLY ALLOWS A SMALL BAND OF THE SPECTRUM OF INCIDENT LIGHT TO PASS. THE DICHROIC MIRROR (B) LEADS THE BEAM THROUGH THE OBJECTIVE TO EXCITE THE SAMPLE. FLUORESCENT LIGHT FROM THE SAMPLE IS COLLECTED BY THE VERY SAME OBJECTIVE, BUT IS ABLE TO PASS THE DICHROIC MIRROR. A FURTHER BANDPASS – THE EMISSION FILTER (C)- BLOCKS STRAY LIGHT.

Separating the fluorescence signal from the illumination is accomplished by a set of filters (Figure 3). The excitation filter allows the entry only from a small band of the visible spectrum. Splitting excitation from the emitted signal is done by a dichroic mirror, which reflects the illuminating beam into the objective but permits the Stokes-shifted fluorescence signal to pass. As the efficiency of the dichroic mirror to block the excitation beam is rather low considering the high intensity of illumination, the stray light is blocked by the so called emission filter. The two filters and the mirror are mounted in blocks – so called filter cubes – that can be inserted in a wheel which makes them easy to exchange.

Usually the filters function as bandpasses for up to four different illumination colors, which allows easy multicolor experiments with all available lasers without the need to switch the filtercube during the experiment.

Upon leaving the microscope via a sideport the emission signal can further be split into spectral channels using the Cairn Research Optosplit which focusses each channel to a different region of the camera chip.

On both setups an Andor Ixon Ultra 897 camera is being used. The camera has an electron-multiplying CCD chip that amplifies the number of photoelectrons at readout, which makes it capable of detecting faint light signals of single molecules.
The imaging process is regulated by a homemade Labview program that controls laser powers and on-times and camera shutters, EM-gain and readout times.
The two setups differ in their extra functionalities: SDT 2 is optimized for fast switching to and from TIRF and is capable of IRM.
SDT 4 is especially well damped against mechanical vibrations to enable simultaneous fluorescence imaging and atomic force microscopy. A wooden box with sound absorbing foam silences acoustic noise and bearing of the microscope on steel cones isolates the microscope from vibrations of the table (Figure 4).

FIGURE 4: A WOODEN BOX (LEFT) DAMPS VIBRATIONS TRANSMITTED VIA AIR. STEEL CONES (RIGHT) MOUNTED UNDER THE MICROSCOPE DECOUPLE IT FROM VIBRATIONS TRANSMITTED VIA THE TABLE.

2.3 TIRF-MICROSCOPY

Total internal reflection fluorescence (TIRF) is an optical near-field phenomenon to investigate cellular and molecular processes at the cell attachment site. It utilizes the phenomenon that a beam of light propagating from a medium of higher refractive index (typically glass) to a medium of lower refractive index (aqueous medium) will by totally reflected at angles larger than the so called critical angle. In such cases only an evanescent wave is able to enter the sample. The intensity of this wave decays exponentially and the excited volume can be confined to a layer typically less than a hundred nanometers away from the glass substrate.

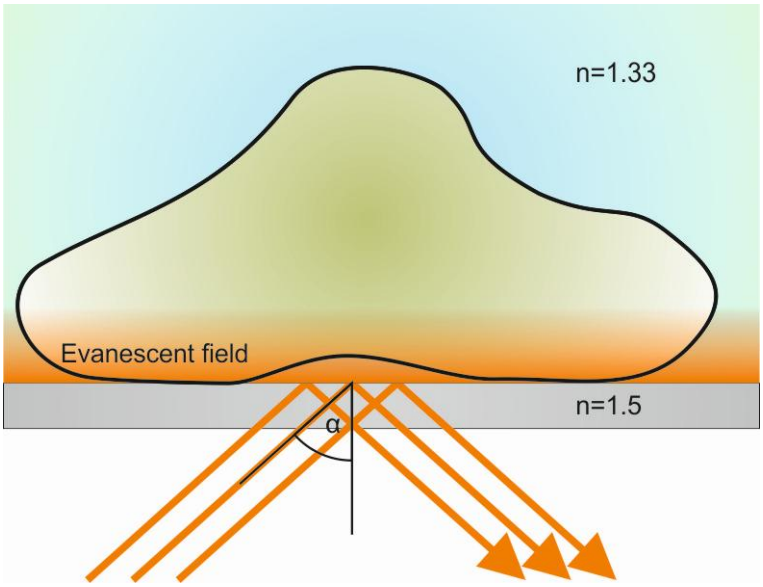

FIGURE 5: WHEN PASSING FROM THE MEDIUM WITH HIGHER REFRACTIVE INDEX (GLASS, N=1.5) TO THE MEDIUM WITH LOWER REFRACTIVE INDEX (WATER, N=1.33) A LIGHT BEAM WITH AN ANGLE OF INCIDENCE α LARGER THAN THE CRITICAL ANGLE IS TOTALLY REFLECTED AT THE INTERFACE. ONLY THE EVANESCENT FIELD IS ABLE TO ENTER THE SAMPLE CHAMBER. AS THIS FIELD DECAYS EXPONENTIALLY ONLY A THIN SHEET (TYPICALLY 100 NM) AT THE INTERFACE IS ILLUMINATED.

In general, for a beam of light propagating from a medium with refractive index n_1 to another medium with refractive index n_2 Snellius' law determines the angle of the refracted beam α_2 depending on the angle of incidence α_1 (both angles relate to the normal of the interface plane):

$$n_1 \sin \alpha_1 = n_2 \sin \alpha_2$$

For $n_1 > n_2$, which is the case for propagation from glass substrate to aqueous medium, incidence angles larger than the critical angle $\alpha_c = \sin^{-1}(n_1/n_2)$ cause α_2 to exceed $\pi/2$, therefore the beam is totally reflected back in the first medium and does not enter the second medium (Figure 5). For interfaces between glass ($n = 1.515$) and water ($n = 1.33$) α_c is 61.3°. Analysis of the electric field using the Fresnel equations, however, shows that the electric field of the light beam is partially able to penetrate the second medium. The intensity of this evanescent field decays with perpendicular distance z from the interface:

$$I = I_0 e^{-z/d}$$

where I_0 is the field intensity at the interface and d is the characteristic exponential decay depth for a given wavelength λ and for given angle of incidence α:

$$d = \frac{\lambda}{4\pi}(n_1^2 \sin^2 \alpha - n_2^2)^{-1/2}$$

This limits the illuminated volume to a thin layer which can be tuned by adjusting the incidence angle. TIRF microscopy is frequently used to suppress unwanted cytosolic background signal when investigating phenomena at or close to the cell membrane, which is of particular

relevance to detect single molecules. Additionally the decrease of total light exposure alleviates phototoxic effects on the cell. The width of the excited layer is usually around 100 nm (1/e), which is less than the PSF in axial direction compared in conventional widefield microscopy.

The intensity of the field at the interface is for the parallel component

$$I_0^{\parallel} = \frac{\left|A_{\parallel}\right|^2 \left(4\cos^2\alpha_1 \left(2\sin^2\alpha_1 - \frac{n_2}{n_1}\right)\right)}{n^4\cos^2\alpha_1 + \sin^2\alpha_1 - \frac{n_2}{n_1}}$$

and for the perpendicular component

$$I_0^{\perp} = \frac{|A_{\perp}|^2(4\cos^2\alpha_1)}{1 - \left(\frac{n_2}{n_1}\right)^2}$$

where $\left|A_{\parallel}\right|$ and $|A_{\perp}|$ are the respective components of the amplitude of the incoming light beam. I_0 can be substantially larger that $|A|^2$, but the time average of energy flow vanishes. Both components undergo phase jumps of different amounts producing ellipsoid polarized light from circular polarized light, the phase difference between both reflected components however vanishes at the critical angle ($\alpha = \alpha_c$) and at grazing incidence ($\alpha = \frac{\pi}{2}$) (Born & Wolf, 1999). The polarization of the evanescent field shows a “cartwheel”-pattern with a spatial frequency of $\frac{\lambda}{\frac{n_2}{n_1}\sin\alpha_1}$ which distuingishes the evanescent field from subcritical refraction.

At the advent of the TIRF technique imaging and excitation pathways were separated (Figure 6, left). The latter consisted of a prism attached to the sample chamber opposite of the objective which allowed coupling the light source into the prism from the side. The disadvantage of this method is that the fluorescence signal has to propagate through the sample chamber prior to detection and can be distorted during the passage. The small working distance of objectives capable of high magnification limits the application of prism-based TIRF as they require an image distance smaller than the thickness of the sample volume and the thickness of the protecting coverslip combined. Furthermore in some designs the prism covers the sample volume, making manipulation difficult.

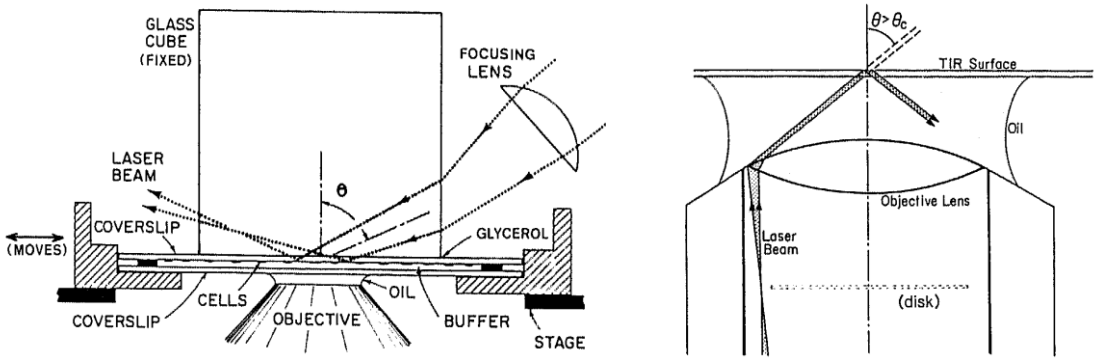

FIGURE 6: EXPERIMENTAL SETUPS FOR PRISM-BASED TIRF (LEFT) AND OBJECTIVE-BASED TIRF (IMAGES FROM (AXELROD, 1989)

The invention of TIRF illumination through the objective (Figure 6, right) made the method far more user-friendly and facilitated single molecule techniques. The excitation light is focused in the back focal plane of the objective, providing collimated light at the exit of the objective. This is crucial for TIRF as all rays should be parallel to avoid partial subcritical incidence. An on-axis light beam will go through the objective in a straight line; if the passage through the back focal plane happens off-axis the beam will be tilted. To shift the position of the beam commonly the last mirror before the beam enters the microscope is turned creating a TIRF pathway diverging from the standard pathway or a mirror is displaced linearly directly shifting the beam parallel to the standard pathway. Objective-based TIRF requires special objectives making it more expensive than the prism-based design. To achieve total internal reflection light has to emerge from the objective in a steep angle. The range of angles the objective can emit light from is characterized by its numerical aperture $NA = n \sin \theta$ where n is the refractive index of the surrounding medium and θ represents one-half of the objective angular aperture. To investigate cells (refractive index of cytosol: 1.38) closely attached to the glass substrate a NA exceeding 1.38 is required. With higher NA the resolution of the objective cannot be enhanced as not more light is able to enter the objective due to the refraction of light at the cell-glass or water-glass interface, however the area in the back focal plane that can be used to create total internal reflection increases, thus making adjustment easier. Steeper incidence angles than the critical angle further allow reducing the penetration depth of the evanescent field. The NA of TIRF-objectives used in practice ranges from 1.44 to 1.7. The latter require high index immersion oil and high index glass cover slips.

2.4 INTERFERENCE REFLECTION MICROSCOPY (IRM)

The TIRF technique runs into trouble when the cell membrane under investigation exhibits ruffles. Even for absolutely homogeneously distributed fluorescent labels secondary structures will appear, which arise from markers in membrane patches not closely attached to the glass substrate being illuminated with less power due to the depth profile of the evanescent wave.

Such an effect would be a serious concern for the micropatterning approach as the fluorescent contrast due to recruitment of labelled protein should not be compromised by cell membrane topography artefacts. To test for that co-staining with a marker that is known to randomly spread in the membrane and looking for clustering is a viable option.

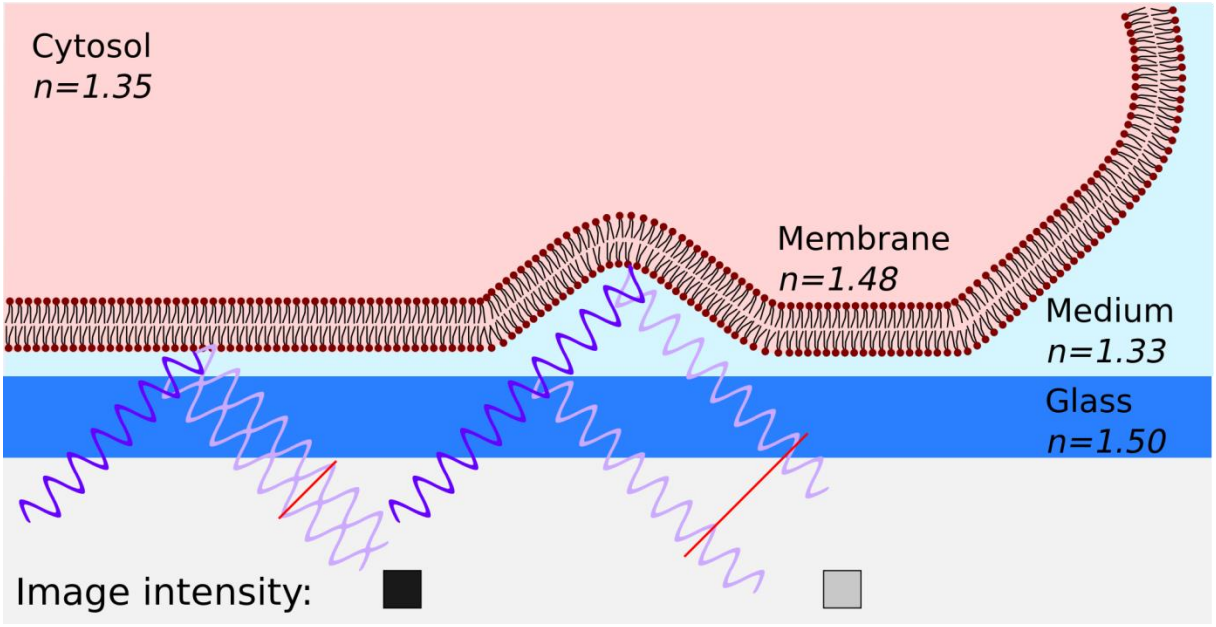

FIGURE 7: A LIGHT BEAM REFLECTED AT THE GLASS – WATER INTERFACE INTERFERES WITH THE LIGHT BEAM REFLECTED AT THE WATER-CELL INTERFACE. THE INTENSITY IN THE IMAGE DEPENDS ON THE GLASS-CELL DISTANCE, WHICH CAUSES PHASE DIFFERENCE. (IMAGE SOURCE:(WIKIPEDIA, 2.12.2014))

We also implemented a complimentary microscopy technique that is able to measure the distance between glass and cell called interference reflection microscopy (IRM) or reflection interference contrast microscopy (RICM) (Figure 7). Before entering the sample volume a fraction of the light is reflected at the substrate/medium–boundary; a further fraction is reflected as the beam passes through the cell membrane. The reflectivity of a beam that is propagating from a medium with refractive index n_1 to a medium with refractive index n_2 is given by $R = \left|\frac{n_1-n_2}{n_1+n_2}\right|^2$ on the assumption of normal incidence. Reflectance or more precisely refractive indices and their changes at interfaces are the only material properties contributing to the image. IRM is a label-free technique and thus not a fluorescence microscopy method. Brightness differences within the image are created by the interference of the two reflected beams. The intensity of the signal is proportional to the distance between substrate and cell membrane. In areas free of attached cells or debris only the reflection of the glass/medium-interface contributes to the signal. Areas brighter than this background are due to positive interference, whereas darker areas are due to negative interference.

The phenomenon of interference can be best explained in the wave picture: Two waves of the same origin don't necessarily overlap when merged again as they have passed through

different optical paths, defined as the product of distance travelled and the refractive index of the propagation medium, and have therefore different phases that determine the physical behavior upon the merger. When crest and through overlap, or more specifically when the optical path difference is an integer multiple of the wavelength of the light beam $m\,\lambda$, optimal conditions for an amplification of the signal are met. This is equivalent to a phase difference of zero. Maximal attenuation is caused by an optical path difference of $\left(m+\frac{1}{2}\right)\lambda$ or a phase difference of π; intermediate values lead to weakened effects. Optical path difference is the additional distance the beam reflected at the water-cell interface has to travel compared to the beam reflected at the glass-water interface, thus it is twice the distance glass – cell. Here only incident light perpendicular to the interface is considered.

An additional optical phenomenon contributes to the formation of the image: Light passing from a medium with lower refractive index to a medium with higher refractive index as it is seen at the cell membrane is shifted by π upon reflection. For monochromatic light as it is used for this study this leads to bright signals for glass-cell-distances $d=\left(m+\frac{1}{2}\right)\lambda/(2n)$ and dark signals for $d=m\lambda/(2n)$ where n is the refractive index of the medium. Cells attaching directly to the surface form dark areas regardless of interference effects as the reflectivity of the system is decreased due to the smaller changes in refractive index in the absence of an intermediate layer of medium with small refractive index (Bereiter-Hahn, Fox, & Thorell, 1979). Cell adhesion studies make use of the smallest orders – dark spots indicate strong adhesion with substrate/cell-distances of below 15 nm, white areas indicate cell media layers of approximately 100 nm, grey areas intermediate values (Barr & Bunnell, 2009) – the identification of higher orders can be somewhat tricky. Using white light and a color-sensitive camera or repeating the experiment with multiple wavelengths allows a combinatorial approach to measure the distance. Using high NA in the imaging pathway diminishes non-zeroth orders as the broad range of angles of incidence cancel out higher orders of incidence (Izzard & Lochner, 1976) and as the depth of focus is reduced (Beck & Bereiter-Hahn, 1981). Reflections within the objective can contribute to stray light unless polarization based antiflex techniques are applied (Ploem, 1975).

Our setup uses a Zeiss HBO 100 mercury short-arc lamp as light source. A Gaussian beam profile and a parallel beam are generated using a spatial filter. A folding mirror overlays the IRM beam path with the fluorescence excitation beam path. The beam is focused at the back focal plane of the objective using a telescope. The second lens of this telescope was shared with the fluorescence excitation beam path in order to save space on the optical table. Overlaying the two beams minimizes required adjustments on the Zeiss microscope. The bright intensity of the mercury lamp is attenuated by a ND 2.0 to allow longer exposure times without overloading the camera. The only further adaption is a special filter cube for IRM

measurements: it contains a single-band bandpass filter to create a monochromatic light beam and a beam splitter. Exposure times were 50-100 ms, electron multiplication at the camera were turned off.

2.5 SUPERRESOLUTION MICROSCOPY

2.5.1 RESOLUTION LIMIT OF CLASSICAL OPTICS

The term superresolution microscopy refers to microscopy techniques that can achieve higher resolution than the classic resolution limit. Due to the diffraction of light a point-like object is imaged according to the point spread function (PSF), which has the shape of an Airy disk. The best resolution of an optical system is given by the distance between two objects at which they could still be distinguished from each other (Figure 8).

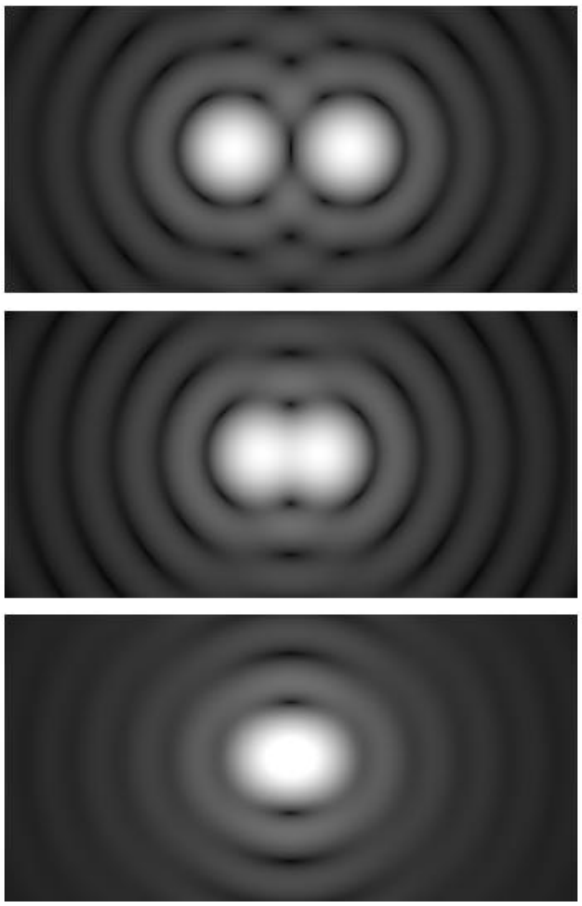

FIGURE 8: COMPUTER GENERATED IMAGES OF TWO AIRY-DISKS. IN THE TOP IMAGE THE OBJECTS REPRESENTED BY THEIR DIFFRACTION LIMITED SIGNALS ARE WELL SEPARATED AND THEREFORE EASILY DISCERNABLE. AT THE INTER-OBJECT DISTANCE DEFINED BY RAYLEIGH'S CRITERION THE TWO OBJECTS CAN STILL BE RESOLVED (MIDDLE). THE OVERLAPPING SIGNALS OF OBJECTS CLOSER THAN THIS DISTANCE ARE SIMILAR TO THE SIGNAL FROM A SINGLE OBJECT (BOTTOM).
SOURCE (WIKIPEDIA)

The Rayleigh criterion defines the ability of resolution if the maximum of the brightness distribution of the first object coincides with the first minimum of the brightness distribution of the second object and vice versa. For a circular aperture the angle at which the first minimum occurs is given by

$$\sin\theta \ = 1.22 \ \lambda/D$$

where λ is the wavelength of light and D is the aperture diameter. The resolution of an optical system is given by

$$R = 0.61\,\lambda/NA$$

where $NA = n \ \sin\vartheta$ is the numerical aperture of the system and n the refractive index of the working medium. The numerical aperture represents the range of wave vectors contributing to the image formation. Following this relation the maximal resolution for a given wavelength is limited by the technical restrictions on the NA of the microscope objective. Using common TIRF-objectives with a NA of more than 1.33 a resolution of 250 nm in the lateral direction is achievable. Further narrowing using specialized high-NA objectives or a confocal setup does not substantially enhance the resolution. For many applications radiation with smaller wavelength (e.g. X-ray, electrons) can be used, but for life cell imaging this is not an option as delicate samples can be severely damaged by the high beam energies.

The first real breakthrough came with Hell's idea to limit the excited volume by using a second, doughnut-shaped laser beam to deplete active fluorophores off the central spot by stimulated emission, hence the name stimulated emission depletion microscopy (STED)(Hell & Wichmann, 1994). Using this nonlinear technique an achievable resolution of 20 nm in the x-y plane in biological systems is reported. (Hell, 2007). STED sparked the development of further techniques that utilize other ways of nonlinear suppression of fluorescence, most notably ground state depletion (GSD) and reversible saturable optical fluorescence transitions (RESOLFT).

2.5.2 LOCALIZATION PRECISION OF A SINGLE FLUOROPHORE

The position of a fluorophore can be determined by deconvolving the image with its point spread function. The PSF of the fluorophore can be approximated with a Gaussian fit, with the centroid of this Gaussian representing the position of object. The precision of the estimation depends on the quality of this Gaussian fit. A simple estimation is given by

$$\langle(\Delta x)^2\rangle = \frac{\sigma^2}{N}$$

where σ in the standard deviation of the point spread function and N the number of photons collected. It is important to have a good optical system to start with small σ; the effect of improvements to existing setups is little as they already work close to the technical limit. It is

fundamental to understand that unlike resolving the signals of two emitters the determination of the position of a single fluorophore is not limited by the diffraction of light but by the finite number of photons. Large efforts are made to increase the number of detected photons. On the one hand this is done by using bright fluorophores, on the other hand by using highly photosensible cameras.

Further errors are introduced by pixelation noise – uncertainties of the exact photon impact position due to the finite size a of the pixels of the camera - and background noise b, which complicates the photon count. The effect of those two factors is considered in Thompson's formula (Thompson, Larson, & Webb, 2002):

$$\langle(\Delta x)^2\rangle = \frac{\sigma^2+a/12}{N}+\frac{8\pi\sigma^4 b^2}{a^2N^2}$$

In practice the localization precision is in the range of 10 – 50 nm, which is significantly less than the diffraction-limited resolution.

2.5.3 PRINCIPLES OF SUPERRESOLUTION MICROSCOPY

The trick of superresolution microscopy is to separately determine the positions of single fluorophores with high localization precision instead of resolving overlapping signals with comparably low performance. To do so it is vital to isolate the signal temporally instead of spatially. Only a sparse subset of fluorophores is activated at a given time so that the nearest neighbor distances are most likely above the resolution limit and fluorophores are therefore easily discernable. The positions are recorded, the fluorophores are bleached during the imaging step and another subset is activated. This imaging/bleaching cycle is being repeated several thousand times. The positions are registered in a two-dimensional histogram with subpixel bin-size. By controlling activating (near-UV) and imaging light intensity and buffer composition it can be ensured that the density of active fluorophores is suitable.

This approach was independently developed by three different groups. Photoactivated localization microscopy (PALM)(Betzig et al., 2006) and fluorescence photoactivation localization microscopy (FPALM) (Hess, Girirajan, & Mason, 2006) make use of photoactivatable or photoswitchable fluorescent proteins whereas stochastic optical reconstruction microscopy (STORM) (Rust, Bates, & Zhuang, 2006) uses organic fluorophore pairs as Cy3 and Cy5; its advancement direct STORM (dSTORM) (Heilemann et al., 2008) uses single organic fluorophores.

Since the advent of single molecule switching techniques, the definition of resolution had to be extended (Shroff, Galbraith, Galbraith, & Betzig, 2008). While in classical optics the discernibility of overlapping signals is crucial, SR adds the density of localizations to the limiting factors. According to the Nyquist-Shannon-sampling theorem two data points per resolution

unit are needed to reproduce the information encoded in the image. The number of collected data points is determined by the finite lifetime of the fluorophores; smearing of images due to thermal drift during the acquisition can be compensated to a certain extent, but ultimately also limits recording time.

During the image reconstruction process signals can be omitted if they cannot be localized precisely enough, the choice for the cut-off has to be balanced as to strict requirements compromise resolution by cutting the number of sample points whereas loose ones might induce artifacts.

2.5.4 FLUORESCENT PROBES FOR SR

The common feature of dyes used in superresolution microscopy is their ability to undergo a transition from an optically inactive to an active state upon illumination at a certain wavelength. This can either be one-way (photoactivation) or reversible (photoswitching). Also transformations that lead to different well-separated maxima in the emission spectrum (photoconversion) can be utilized. Ideally the fluorophore is very bright. The issue of photostability is less crucial compared to other microscopy techniques as the fluorophore is intentionally bleached, however the combination of fluorophore lifetime and brightness should allow recording a sufficient number of photons to obtain a sensible localization precision. On the other hand a too stable fluorophore will compromise the image acquisition time if the illumination power is not high enough to bleach the fluorophore in the desired time. The collective fluorescence from dark molecules might obscure the signal of a single bright one, therefore on the part of the fluorophore a high contrast ratio, which is defined as the emission intensity ratio between dark and bright states, is desired. The activation mechanism has to work in a reliable way; the light controlled activation rate must be high compared to the spontaneous activation rate. From the sample point of view unwanted autofluorescence has to be minimized (Fernandez-Suarez & Ting, 2008).

SR techniques can be classified by the way the protein of interest is labelled. (F)PALM utilizes fluorescent proteins that can be genetically encoded attached to essentially every protein. mEOS3.2, the FP of our choice, was engineered from a protein originating in the stone coral *Lobophyllia hemprichii (Zhang et al., 2012).* This mutant exhibits the photoactivation ability upon illumination with near-UV light which is the essential condition for superresolution imaging.

The essential characteristic of (d)STORM is the use of synthetic fluorescent markers. In the initial proposal of the method the cyanide Cy5 was combined with Cy3, a secondary chromophore that facilitates the photoswitching process. dSTORM extends the method to the implementation of conventional single fluorophores by a controlled induction of off-states using a special buffer system.

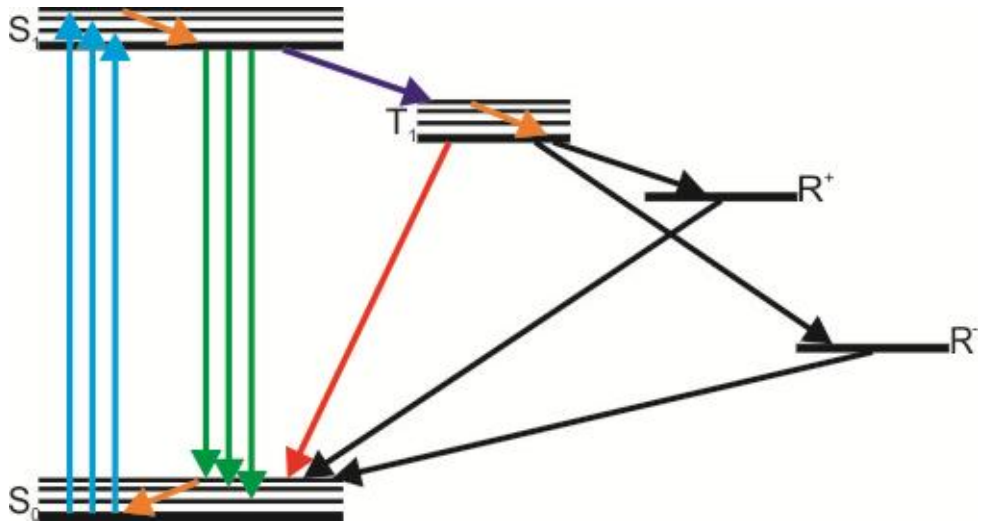

FIGURE 9: JABLONSKI DIAGRAM DEPICTING THE PHOTOPHYSICS OF FLUOROPHORES. IN ADDITION TO THE TWO-LEVEL SYSTEM (S0 AND S1) NEEDED FOR FLUORESCENCE THE SCHEME INCLUDES A LONG-LIVING TRIPLET STATE (T1) THAT IS PRONE TO PHOTOBLEACHING. THE ROXS BUFFER DE-EXCITES THIS STATE TO RADICAL STATES.

The buffer called ROXS contains reducing agents and oxygen depleting constituents. . To explain its principle of operation the simple model from section **Error! Reference source not ound.** has to be extended with a triplet state T1 and redox states. An excited molecule either can go under emission of fluorescence radiation from S1 to S0 or via radiationless intersystem crossing to T1. As the decay to ground state requires a spin flip and is therefore unlikely T1 has a long lifetime. T1 is the state believed to be the main pathway for photobleaching, especially in the presence of oxygen. The idea behind the ROXS buffer is to facilitate an additional de-excitation pathway by depopulating the reactive triplet state by reducing or oxidizing the molecule and then bringing the radical ion to the ground-state by the complementary redox-reaction (Figure 9). Initial reduction is here more likely than oxidation (Beaumont, Johnson, & Parsons, 1997).

This dramatically increases the number of photons emitted before photobleaching and allows more S0-S1 cycles, increasing overall brightness. The lifetime of the radical ion states can be significantly higher than the lifetime of triplet states, making it suitable for stochastic readout. By varying the reductant concentration the average on- and off-times of the fluorophores can be controlled allowing an adaption of the buffer to labelling density, image acquisition time and illumination power so that sufficiently well-separated signals are recorded per single image. Large scale screening proofed thiol-containing substances to be good reagents to reduce the fluorophores to radical anions, the fluorophore is then recovered upon oxidation by remnants of molecular oxygen in the buffer. Both processes, reduction of the triplet state and oxidation of the intermediate reduced state, are facilitated by irradiation, in our case a laser with 405 nm wavelength. Our buffer contains 50-100 mM cysteamine as a reducing agent and 20% glucose, 500 µg/ml glucose oxidase and 40µg/ml catalase as oxygen scavanger.

2.5.5 SHORTCOMINGS OF LOCALIZATION BASED SR TECHNIQUES

Due to the stochastic photochemical behavior of the inactivation process fluorophores (especially organic dyes) are likely to have multiple appearances during a recording session, so that a single fluorophore might appear as a nanocluster of successful localizations whose size depends on the localization precision. Unknown labelling stoichiometry aggravates the problem of calculating the number of targets. An estimation of the number of occurrences of signals linked to one probe can be made by comparing the sample to a test sample prepared with well separated labels, e.g. by immobilizing the probe in a diluted solution on a glass surface. One has to bear in mind that this setting might not represent the situation in the actual measurement as far as the photochemical and photophysical processes the fluorescent label is sensitive to are concerned.

The benefit of spatial resolution is bought at the high price of low time resolution. Acquisition times of tens of seconds only allows the measurement of slow processes by binning raw images; fast dynamics in the range of a few seconds and below have to be prevented by fixing the cells.

The disadvantage of the humanly unintuitive way of image creation should not be underestimated. For example, it is impossible to discriminate the recorded protein localizations from unbound label diffusing through the region of interest.

2.6 ATOMIC FORCE MICROSCOPY

Atomic force microscopy (AFM) is a non-optical imaging technique for surface characterization. The technical foundation of AFM was developed for the scanning tunneling microscope (Binnig & Rohrer, 1986): The probe consists of a cantilever with a sharp tip on its non-fixed end, that acts as a plate spring. An object close to it will interact with the very tip region and due to the force, which is therefore applied to the cantilever, the cantilever is being deflected (Figure 10). The extent of the deflection is a measure of the force and its underlying physical properties. Using piezoelectric elements, the surface can be scanned with very high precision, so that in special cases two-dimensional images with atomic resolution are obtainable.

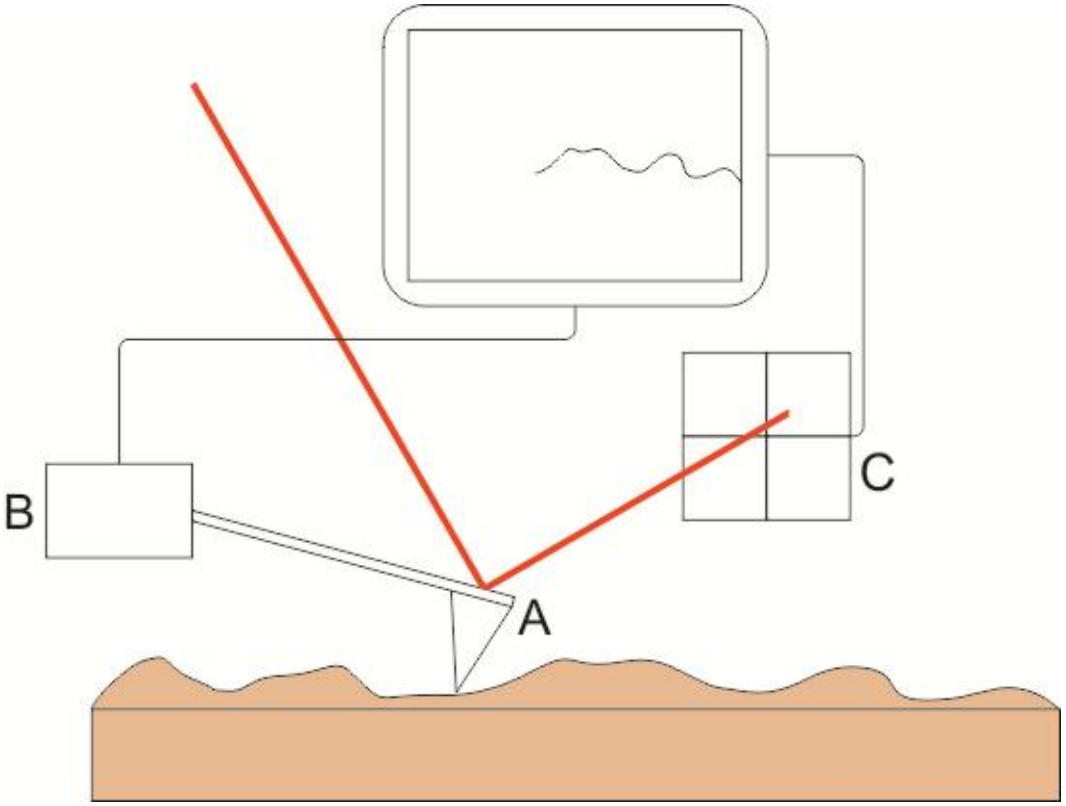

FIGURE 10: AFM. A CANTILEVER (A) WITH A SHARP TIP ON ITS END IS MOVED ALONG A SURFACE BY USING PIEZO ELEMENTS (B). DUE TO INTERACTION OF THE TIP WITH THE SURFACE THE CANTILEVER IS DEFLECTED. THIS DEFLECTION IS DETECTED BY A LASER REFLECTED FROM THE BACK OF THE CANTILEVER ONTO A 4-SEGMENT PHOTODIODE (C). COMBINING LATERAL INFORMATION FROM THE PIEZO ELEMENTS AND HEIGHT INFORMATION FROM THE PHOTOCURRENT YIELDS IMAGES OF THE SURFACE TOPOGRAPHY.

The kind of force that is measured depends on the tip's susceptibility for the force. Protein-protein interaction can for example be measured by coating the tip with one protein and probing a surface covered with the other one. Inert tips as those that are used for this thesis are useful for characterizing the topology and elastic properties of material deposited on a surface.

There are several ways to measure the deflection of the cantilever; most commonly the beam deflection method is used. A laser beam directed at the back side of the cantilever is reflected on a quadrant photodiode so that all four parts of the diode are illuminated evenly if the cantilever is not bent. A deflection of the cantilever redirects the beam, resulting in one part of the diode collecting more photons than the rest. The force applied to the tip can then be calculated from the ratio of photocurrents. The quadrant diode does not only allow detecting the vertical deflection but also the lateral twisting of the cantilever.

The cantilever is usually a rectangular or triangular piece made of silicon or silicon nitride mounted on a chip; it carries a pyramid or a cone with a sharp tip. The sensitivity of the system is determined by the cantilevers spring constant k. The dependence of the force F on the

extension s can be described in a first order linear approximation by Hooke's law:

$$F = -k \, . s$$

Commercially available cantilevers have spring constants in the range of 0.001 N/m to100N/m. The calibration of cantilevers is generally difficult as they are specified by the manufacturer with an uncertainty of up to 20%, material fatigue or modifications to the cantilever further alter the spring constant. Cantilevers with small spring constants, which are used here, can be characterized using a thermal noise analysis method (Hutter & Bechhoefer, 1993).

The resolution of AFM depends on the sharpness of the tip, apex radii of $2 - 10$nm were used for this study. Unfortunately the tips are rather prone to contamination. A reliable way to measure the tip size is electron microscopy. It should be noted that due to tip convolution AFM tends to underestimate area values.

Different modes of controlling the cantilever are available:

In contact mode the tip is kept in touch with the surface. In constant height imaging the tip is scanned over the surface and the deflection of the cantilever is directly used to image the topography. It is also possible to tune the height of the cantilever with a feedback loop so that the force, which the tip applies to the surface, stays constant. This contact imaging mode is often preferred as artifacts caused by the force induced deformation of the object can be minimized.

Dynamic imaging modes excite the cantilever to oscillate at a frequency close to its resonance frequency and scan the surface. Attractive and repulsive forces change the oscillation characteristics of the system. The amplitude and the phase difference of the oscillation of the cantilever compared to the oscillation of the piezos, which drive the cantilever movements, are used to compose an image of the object's surface. The dynamic modes can be subdivided into further categories:

In non-contact mode the tip is separated from the surface by a distance of up to $10\ nm$. In life sciences non-contact mode is uncommon as intermediate fluid layers strongly influence the measurements. Force modulation mode works in the quite opposite regime. This dynamic form of contact mode probes the sample's elastic properties by firmly touching its surface with the oscillating cantilever.

Maybe most used is tapping or intermediate contact mode which would allow the tip to transiently touch the object. Compared to contact mode tapping mode induces less lateral disruption, but it is more susceptible to complications in case of sticky samples.

2.7 MODEL ORGANISMS – CELL LINES

The need for organisms that are uncomplicated to handle and offer robust findings resulted in the development of techniques that could grow cells for prolonged periods in vitro under a well-controlled environment.

The isolation of primary cells from living animal tissue can be a sophisticated process, which has to be repeated numerously since – unless they are stem cells – normal cells cease to divide after a number of cell divisions. The original solution to this problem is to use cells originating from cancerous tissue, where the cell suicide mechanism is deregulated, which allows the cells to proliferate in vitro.

Unlimited reproduction allows establishing the entire cell population from very few or even single cells that exhibit certain wanted properties. So an analysis can be performed several times on genetically very similar cells. This high degree of repeatability is not given for primary cells, however, care has to be taken when interpreting data from cell lines. Mutations responsible for the immortality or mutations that gave the cell survival benefits in the cell culture environment might have led to a loss of the functionality.

Jurkat (Schneider, Schwenk, & Bornkamm, 1977) is a human T lymphocyte cell line from the blood of a T cell leukemia patient; it is commonly used to study T cell signal signaling. Its derivative, the JCaM1.6 cell line is Lck deficient; generally, Jurkat cells – although being CD4-positive – express only low amounts of CD4. The T24 cell line (Bubenik et al., 1973) is a human bladder carcinoma cell line that does not contain endogenous CD4 and Lck. The natural lack of the proteins CD4 and Lck in the cell lines used makes sure that only the proteins of interest, which are modified for the experiment, are expressed. The alterations on the proteins are attachments of fluorescent proteins to visualize the position of the protein, but also mutations that for example affect binding sites and therefore probe the molecular interaction mechanisms are common.

At the beginning of this thesis DNA sequences of human CD4 and human Lck-mEOS3.2 were in stock, but cell lines permanently expressing both were not established. In the first step recombinant DNA had to be created. These are plasmids – DNA ring structures that encode both the DNA of the proteins that should be expressed by the cells, as well as additional DNA sequences facilitating the expression of the inserted protein.

The vector is modular. It contains several restriction recognition sites – nucleotide sequences that are recognized by enzymes that specifically cut them. Usually these short sequences are palindromic, so that after the cut an overhang remains (sticky end). The DNA encoding the protein of interest contains complimentary overhang and thus be the ligated to the plasmid. To have enough protein to work with the number of proteins strands was amplified by PCR prior to the ligation.

In the transformation step plasmids are mixed with competent E. coli, which take up the plasmids. The plasmid also carries a sequence that makes the bacterium antibiotic-resistant. Plasmid positive colonies can thus easily be spotted when the bacteria solution is spread out on ampicillin containing culture plates. Single colonies – originating from a single bacterium and therefore genetically identical – are then expanded in media, harvested and lysed. Due to this amplification step large quantities of DNA can be extracted from the lysate using purifying kits that bind DNA.

The vector contains virus-derived DNA. When a cell is transfected with the plasmid it will produce viroid particles containing the DNA of the protein of interest but not the DNA required for virus replication. We used the HEK (human embryonic kidney) cell line to produce virus particles. Supernatant medium containing the medium was then finally transferred to the cells which should be transfected.

All steps have to be monitored. The size of plasmids and DNA fragments is determined in-house with gel electrophoresis, the exact sequence by specialized companies.

As not all cells can be transfected or as the ability to express the proteins of interest might be lost over time, the cells have to be screened and sorted. In FACS (Fluorescence assisted cell sorting) machines single cells are illuminated by laser light. The brightness of the fluorescent signal at various wavelengths depends on the abundance of the protein of interest, which is either intrinsically labelled by a fluorescent protein (hLck-mEOS3.2) or externally labelled with fluorophore-linked antibodies prior to cell sorting (CD4). From light scattering conclusions on cell size and cell health can be drawn. The cell solution jet is spread into charged droplets containing single cells. By applying an electric field the trajectory of the droplet can be steered into different bins and individual positive cells can be separated from cells without the desired proteins and properties.

2.8 SOFT LITHOGRAPHY FOR CREATING PROTEIN STRUCTURES

Soft lithography is a printing technique that is able to deposit proteins in well-defined micrometer scale patters. The imprint process doesn't require a clean-room environment and is therefore cheap in relation to photolithography, which is the dominant technique in semiconductor fabrication.

Compared to other deposition methods like dip-pen lithography using AFM, e-beam lithography and additive manufacturing methods (stereo lithography, two-photon lithography, STED lithography), soft lithography has the advantage of creating structures up to the extent of a few square centimeters in a single step, therefore it is a very fast technique. Creating structures using additive manufacturing techniques requires monomers that are polymerized after illumination only if a special photoinitiator is present. Functional groups in the polymer

then mediate the protein's attachment to the structures. With this technique manufacturing of flat monolayers is not possible.

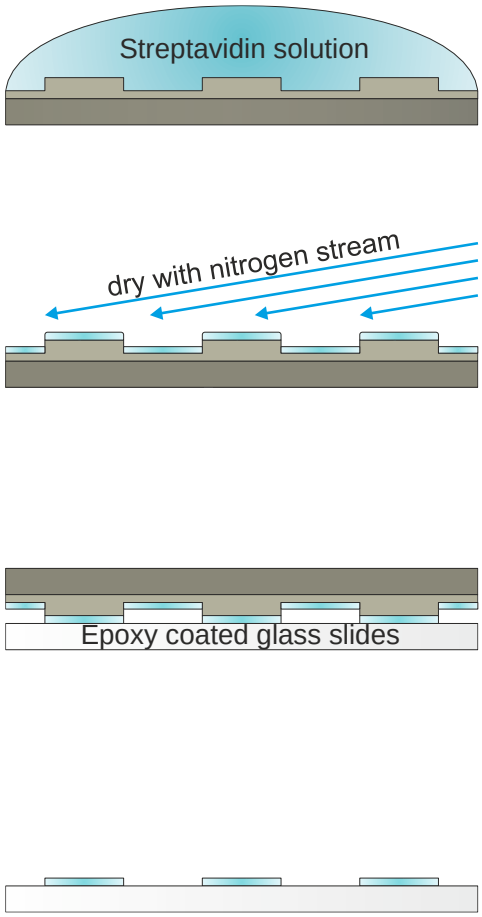

FIGURE 11: THE IMPRINT PROCESS. STREPATVIDIN CONTAINING SOLUTION IS INCUBATED ON THE STAMP SO THAT A THIN LAYER OF PROTEIN FORMS AT THE INTERFACE. RESIDUAL SOLUTION IS REMOVED BY A NITROGEN STREAM OR BY SPINCOATING. THE STAMP IS THEN PRESSED ON THE GLASS SUBSTRATE, THEREBY TRANSFERRING THE PROTEIN FROM THE STAMP TO THE SUBSTRATE.

The most common soft lithography method is microcontact printing (µCP) (Figure 11). The fabrication of the stamps is split into two processes. At first a master stamp has to be produced using photolithography (feature sizes $> 1\ \mu m$) or e-beam lithography (feature sizes $> 20 - 30\ nm$) (Qin, Xia, & Whitesides, 2010). This step requires clean-room conditions and highly developed equipment, however, only one single master is required. All further workflow, activities that are done not only once but in everyday work, can happen in normal lab environment. The key element of soft lithography is an elastomeric stamp. It can be produced by casting a liquid precursor against the master's complementary structures, curing it and then peeling it off. As the stamp is very soft compared to the master, the master is not damaged by the procedure and can be used multiple times. In non-cleanroom conditions the master will inevitably be contaminated by dust particles. This does not damage the master as the particles are incorporated in the work stamp and are removed with the peel off, thereby cleaning the master.

Further requirements are easy processing, wettability ideal for protein transfer and nontoxic properties are desired. Polydimethylsiloxan (PDMS) is widely used for this purpose. The quality of the imprint is determined by the material's ability to make conformal molecular level contact to the substrate, so soft materials are preferred. On the other hand the resolution is limited by sagging of the recessed regions and by lateral deformation of the structures. Sagging can be alleviated by attaching the elastomer on rigid substrates, lateral deformation can be countered with lower aspect ratios of the structures on the stamp or with harder materials. PDMS provides excellent results for feature sizes larger than $1\ \mu m$, smaller structures, however, require novel materials.

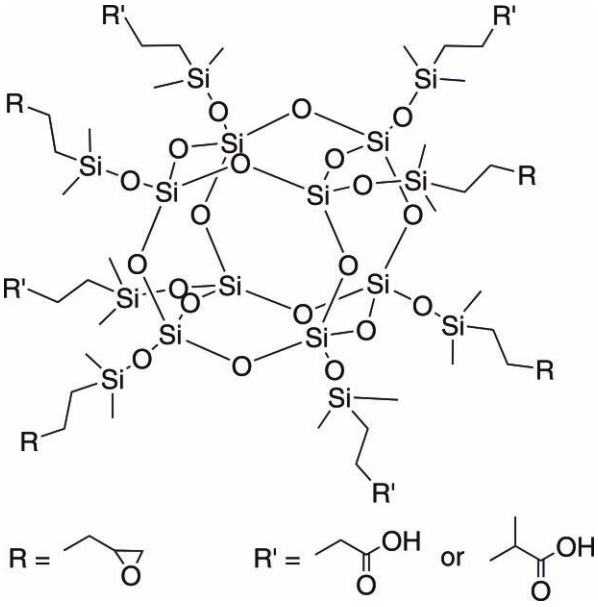

FIGURE 12: STRUCTURE OF A POSS MONOMER AND FUNCTIONAL GROUPS (R - EPOXY GROUP, R' – CARBOXYLIC GROUP).

Our industrial partner introduced polyhedral oligomeric silesquioxane (POSS) into contact printing (Kastner et al., 2014). POSS is a nanoparticle with a cage-like silica core with functional groups such as epoxy-carboxylic acid groups attached to the eight corners (Figure 12). These functional groups on the one hand link the particles to each other and on the other hand they can increase protein binding to the stamp. Both processes can be tuned by varying the amount of functional groups during the synthesis. Furthermore the epoxy groups conjugated with the adequate photoinitiator allow the resist to solidify within seconds under UV-illumination at room temperature.

2.9 PROTEIN-PROTEIN INTERACTION

Cellular processes rarely depend on the action of single proteins, but on the specific formation of complexes of various protein molecules. Physiological cell processes such as signaling are enabled by the interplay of numerous co-partners – each participating protein has a very

specialized and limited molecular function. Methods to investigate these interactions are usually based on testing the mutual binding affinity of proteins that are suspected to play a role in the process.

Several in-vitro biochemical assays are known, most notably co-immunoprecipitation (Phizicky & Fields, 1995). Also measurements of the change of the optical properties upon binding is common (Stahelin, 2013).

Investigations in live cells can be done by fluorescence resonance energy transfer (FRET) or fluorescence cross-correlation spectroscopy (Eigen & Rigler, 1994); these ensemble methods perform well in case of proteins with high binding affinities.

To capture the spatiotemporal distribution of membrane proteins multicolor imaging is a very useful approach. After compensation of the chromatic aberration of the imaging system by thorough calibration the intensity distributions of the color channels which map the location of the corresponding labelled proteins can be correlated. A large problem in the analysis of the images is coincidental overlap of the fluorescent signals. For a small number of labelled proteins this overlap can be calculated and the analysis can be adjusted accordingly, densely crowded membranes however pose a problem.

A few techniques have been devised to overcome such limitations. One approach is to limit the number of active labels in the measurement area. Using a two-color TOCCSL (thinning out clusters while conserving the stoichiometry of labelling) (Ruprecht, Brameshuber, & Schütz, 2010) protocol all fluorophores in one part of the cell membrane are being bleached. Proteins labelled with an active fluorophore diffuse from the non-illuminated part of the cell, which acts as a reservoir, into the measurement area. The diffusion process is sufficiently slow to be able to record the influx of single protein complexes to the imaged region, so the tracks of the protein of interest and of its putative interaction partner can be followed. Motion in pairs is a very strong indicator for protein-protein affinity. An inherent shortcoming of this method is the inability to track stationary proteins and its bias towards the fast moving fraction of heterogeneous populations of protein complexes.

Signal overlap can be mitigated by using superresolution imaging. The more precise localization of the interaction partners eases assignment. Microscopy setups using STED and similar techniques are usually built to support only a single excitation wavelength, as even for single color imaging multiple wavelengths (excitation and STED) are involved. The usage of dyes that nevertheless have discernable emission spectra due to largely differing Stokes shifts (Schmidt et al., 2008) or that exhibit a difference in their fluorescence lifetime have been reported (Bückers, Wildanger, Vicidomini, Kastrup, & Hell, 2011). Technical requirements for implementing multicolor images on STORM and PALM setups are low and only require suitable

lasers and beamsplitters. As image acquisition times are relatively high detecting transient binding can be challenging.

All colocalization techniques share the problem of chromatic aberration. Overlaying images of different color require proper calibration and shifting and stretching images accordingly. Excitation of fluorophores with different wavelengths can have unwanted effects on their lifetime. Especially the performance of the long-wavelength dyes can be limited upon irradiation only suitable for the excitation of the short-wavelength label.

2.10 Interaction assay based on protein micropatterning

2.10.1 The Idea

The assay proposed by our group in (Schwarzenbacher et al., 2008) can circumvent some of the major difficulties of optical colocalization methods by preparing the sample in a way that exact two-color overlays are unnecessary and no special optical equipment is needed. It is still based on colocalization, however, in this assay it is a priori known that one of the interaction partners (termed bait) is spatially enriched in a highly regular pattern given by the experimentalist. If the other interacting, labelled molecule (termed prey) follows this pattern the location of bait-rich and bait-depleted areas can be easily deduced in one measurement of the prey without the need to label the bait (see Figure 13).

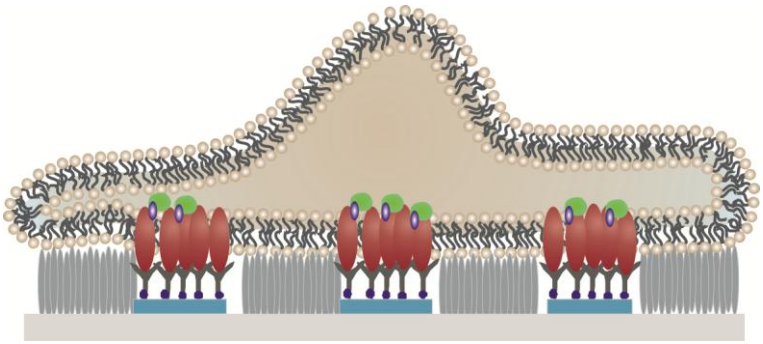

Figure 13: Antibodies linked to Streptavidin structures enrich the bait protein (red) in certain domains in the cell membrane. Due to protein-protein interaction the prey protein (blue), which is fused to a fluorescent protein (green), colocalizes with the bait.

The degree of affinity can be determined in a very easy fashion by comparing the density of the recorded molecule on-pattern versus off-pattern. A refined approach is to track single prey molecules. A change in diffusion speed or transient stops of diffusion in bait-enriched zones can yield valuable information on protein-protein interaction kinetics.

Binding mechanics can then be tested by investigating the influence of system alterations on the outcome of the experiment. These changes of the system can for example include selective

mutation of proteins to erase binding domains in the amino acid sequence, depleting certain lipids in the plasma membrane, or degrading the cell's actin cytoskeleton.

2.10.2 PREREQUISITES

The experimental challenge that arises is the creation of protein-enriched and protein-depleted areas in life cell membranes. To do so the exoplasmic domain of the protein of interest is targeted by a corresponding antibody, which, in turn, is anchored to a solid substrate. The substrate is a glass cover slip with functionalized coating that binds streptavidin (SA). SA is a 52.8 kDA homo-tetrameric protein produced by the bacterium Streptomyces avidinii that has a strong affinity to bind the small ligand biotin (244 DA). This bond is known to be one of the strongest non-convalent interactions in nature and is therefore extensively used in biotechnology. Many biotinylated antibodies are offered and can so be linked to streptavidin to complete the chain.

The intermediate SA-biotin link has numerous advantages. First it is cheap compared to the antibody. At the substrate deposition step the protein is used in excess. Most of it is lost in the printing process, and only a monolayer of the protein is supposed to be transferred to the glass substrate. Streptavidin is a rather robust protein that withstands the harsh non-physiological chemical conditions during the deposition more easily than other proteins. It can also be dried for storage and transport. Moreover, the system is very versatile and allows to investigate a variety of membrane proteins.

With the biotechnology available the task of making patterns of proteins within the cell membrane is translated to creating patterns of SA on glass substrate that serves as a template for the distribution of the targeted protein in the plasma membrane.

3 METHODS

The main focus of this thesis is the quality control of the protein structures during the establishment of a protocol to create patterns with feature sizes close to or below the classical optical resolution limit. The task is to identify desired and unwanted properties and to correlate their appearance to parameters of sample preparation, transport and storage.

The main tool to gain knowledge on the quality of the structures is TIRF-microscopy. It lacks the resolution of AFM and optical superresolution techniques but allows for fast image acquisition and therefore enables the investigation of large areas of supposed protein deposition making it the preferred method to gain a general overview over a large number of samples. Typical times of 1-5 ms of sample illumination and 30 ms for whole camera chip readout are negligible compared to the time the microscope user needs to find a suitable spot for representative images.

AFM and superresolution microscopy will be essential when progressing to feature sizes below the diffraction limit, in the scope of this thesis they were used to obtain high-resolution information on the substructure of the lines. AFM provides knowledge on the topography of deposited, but not on its functionality, which is supplemented by dSTORM.

3.1 LABELLING

As small Streptavidin structures are not visible in light microscopy they have to be labelled by a fluorophore. We incubated a solution of biotinylated antiCD4-antibody and BSA on our structures for 15 minutes. The antibody binds to the structures and BSA passivates the glass surface thereby blocking remaining functional groups. After washing with PBS a secondary Atto 647N-labelled antibody that binds to the antiCD4-antibody was added.

To contain liquids on the sample SecureSeal Hybridization chamber, which have a plastic sheeting that covers the sample volume, were used. For AFM experiments the sample area was enclosed by a barrier made of picodent twinsil two-component adhesive.

3.2 QUANTIFICATION OF FLUORESCENCE IMAGES

In order to compare different protocols for pattern creation the final results were characterized by parameters that quantify the quality of the structure. I chose those parameters to meet the requirements needed to successfully apply the nanostructures in cell experiments.

Meso scale

Not all cells might show the behavior of interest, therefore it is often necessary to be able to choose small subsets. As far as the experimental platform is concerned this means that the area on which nanopatterns can be found has to be reasonably large so that a sufficiently large amount of suitable cells is provided. Another simple but nevertheless important aspect is that larger areas are easier to find on the glass substrate. One has to keep in mind that forcing cells to interact with patterns and the exposure to the harsh conditions on the microscope in general might induce unwanted effects that increase with time. It can be vital to find the experimental area within a short time after cell spreading even with high magnification objectives (field of view <100 x 100 µm).

Micro scale

Pattern-based experiments rely on the comparison of cell properties on- and off-pattern. No bias should be induced to the experiment by neighboring structures with different properties. This would not only increase the deviation in the outcome of whole cell experiments; probing the nanoscale compartmentalization of the cell membrane would be futile if effects due to inhomogeneities of the platforms are larger than due to biological reasons.

Nano scale

A further important property is the density of functional proteins within the structures. Performing tests on high density structures yields better on-/off-pattern contrast ratios and enhances the dynamic range of the experiment. Scaling the activity of the pattern is better done by diluting the micropatterned ligand (i.e. the biotinylated antibody) with non-active ligand (free biotin) than by varying the density of deposited material (SA), as it tends to agglomerate instead of spreading evenly.

The quality of the patterns was rated separately in those three abovementioned fields. Image evaluation by computational means proved to contain various imponderabilities, most of all inhomogeneous sample illumination on different setups over a time period of one and a half years, so the patterns were graded by human eye in a 0 to 3 points system for every field. The final score is the sum of all three categories.

Examples of successful imprints and their rating can be seen in Figure 14.

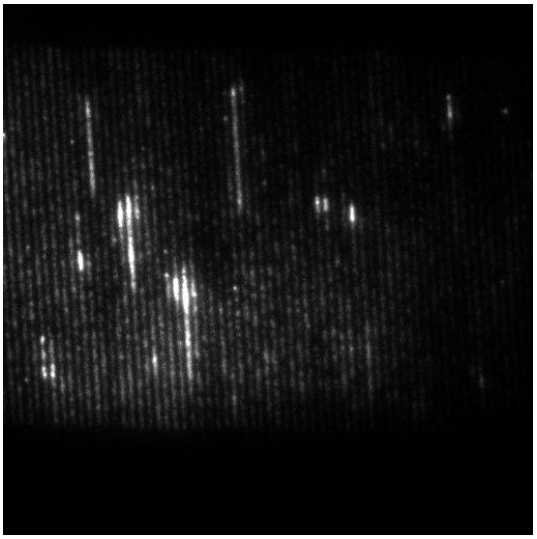

3/1/3: Small regions of very dense lines.

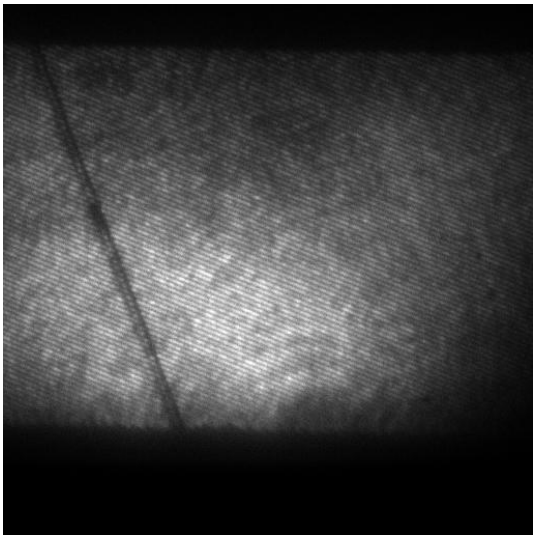

3/3/3: Large area of nearby lines having similar high brightness levels. Inhomogeneities in the image arise from imperfect illumination

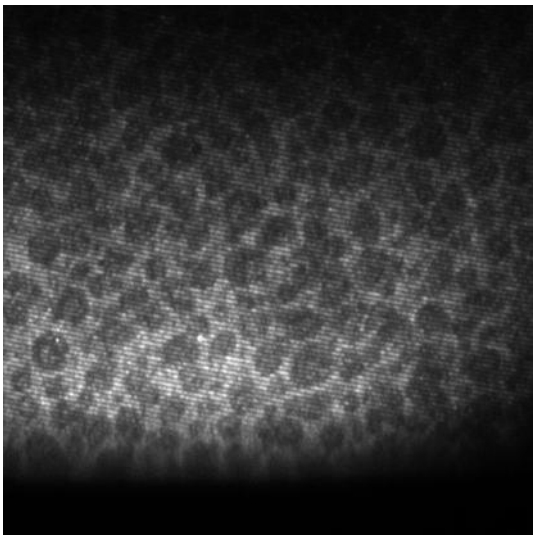

2/2/3: „Leopard skin“-patterns can be frequently seen.

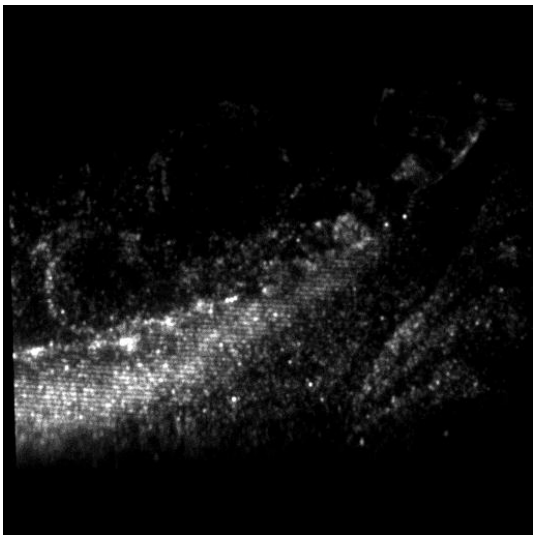

3/2/1: Reasonably bright lines. The total area of structures is very small.

FIGURE 14: EXEMPLARY FLUORESCENCE IMAGES AND GRADING. THE NUMBERS ARE THE RATINGS FROM 0 (NO STRUCTURES AT ALL CAN BE SEEN) TO 3 (BEST) FOR NANO SCALE / MICRO SCALE / MESO SCALE.

The division into three categories reoccurs in the presentation of the analysis of the imprint parameters in section 4, where in addition to the total score they are separately shown (nano: top right, micro: bottom left; meso: bottom right).

4 RESULTS

4.1 MATERIALS

4.1.1 GLASS SUBSTRATE

The application of our structures in fluorescence microscopy requires the usage of thin glass coverslips to support the protein lines. Conventional untreated glass does not exhibit protein affinity which is high enough to reliably attach proteins in aqueous environment and under traction applied by cells, so we tested different kinds of surface functionalizations and surface treatments to enhance protein binding (Figure 16).

Previous studies performed in our lab used Schott Nexterion-E glass coverslips, which are covered with epoxides, functional groups that consist of cyclic ether with three ring atoms. This ring exposes the oxygen in the molecule which makes it more reactive than the stretched ether form. Epoxy covalently binds to nucleophilic amine-, thiol- or hydroxyl groups provided by the amino acid side chains of the deposited protein. The protocol used for micropatterns with PDMS suggested rinsing epoxy-coverslips with ethanol and deionised water prior to use.

Schott Nexterion-A coverslips provide similar function. They possess an aldehydesilane coating that bonds to NH_2-groups in the protein. We also tried Schott Nexterion-H coverslips that use NHS-ester to provide binding to amino groups.

Proteins can also bind electrostatically to glass-slides, however the durability of this bond was not known. To increase surface charges coverslips were treated with oxygen-plasma or with piranha solution (a very reactive mixture of 50% H_2SO_4 and 50% H_2O_2 – make sure to use suitable safety equipment). Plasma slides were freshly prepared before the imprint, piranha slides one day beforehand.

We also tested indium tin oxide (ITO) covered surfaces. These are an intermediate product in the production of functionalized surfaces.

4.1.2 PROTEIN

Linking antibodies to Biotin is a common technique, and a large variety of Biotin-tagged molecules is commercially available. A couple of substances are known to show strong affinity to bind Biotin, amongst which Avidin (pure, mixed with Streptavidin, labelled with FITC fluorophore) was used in preliminary studies. Streptavidin has a more preferable isoelectric

point, lower nonspecific binding and was successfully used with PDMS stamps. Therefore the system was optimized for this protein (Figure 17).

The first essential step for a successful imprint is the formation of a monolayer of protein on the stamp. The following requirements have to be taken into consideration: The size of the liquid drop that is needed to cover the whole printing area is defined by the curvature of the drop due to its surface tension. Enough protein to cover the stamp surface has to be in the solution. Excess protein is washed away. We tried to minimize this loss while preserving a sufficient amount of Streptavidin on the stamp (Figure 18).

It has to be noted that the stated concentration is derived from the nominal value of protein in the vile that was shipped by the vendor and the amount of PBS it was solved in. Protein loss during handling and storing was not accounted for.

4.1.3 BUFFER

The functional integrity of streptavidin is best preserved in media with physiological salt concentrations like Dulbecco's phosphate buffered saline (PBS). We tested several buffers with varying supplements and acidities (Figure 19). The documentation of buffers used for this study is not published yet.

4.1.4 STAMP

Eight available sites to link functional groups to POSS nanoparticles allow customizing the physical properties. We used epoxy-hexene, allylacetic acid and methylallylacetic acid in varying ratios (Figure 20). Details on the synthesis can be found in (Kastner et al., 2014). For this thesis mainly a stamp design of lines with linewidth 230 nm and 500 nm period was used. Imprints with smaller feature sizes (NILT 1041) have preliminary character.

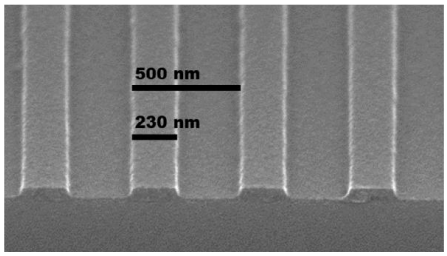

FIGURE 15: SECONDARY ELECTRON MICROSCOPY IMAGE OF POSS STAMPS (KASTNER ET AL., 2014).

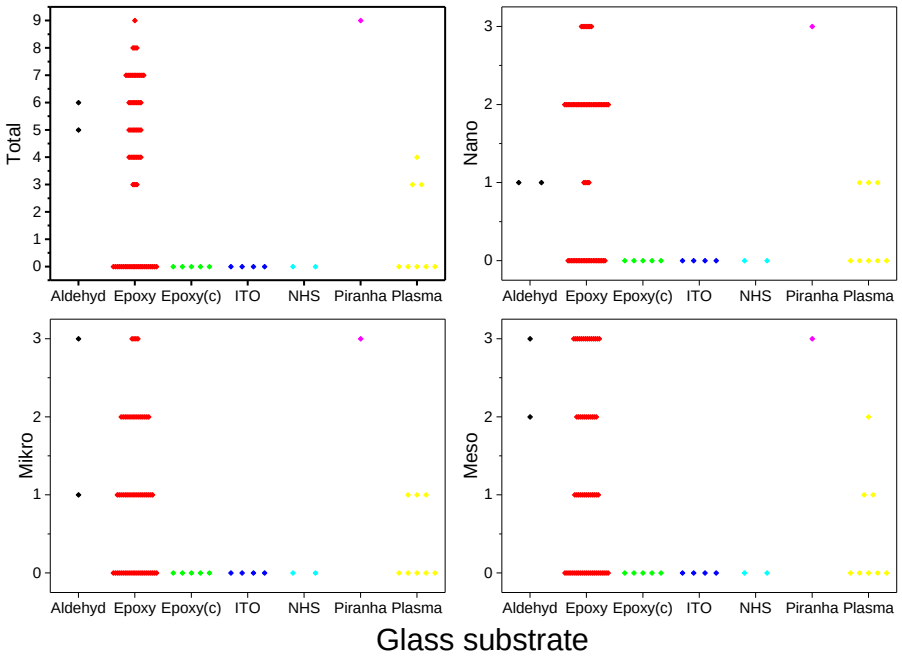

FIGURE 16: QUALITY OF IMPRINTS FOR DIFFERENT CHOICES OF GLASS SUBSTRATE (ALDEHYD – SCHOTT NEXTERION AL, EPOXY –SCHOTT NEXTERION E, EPOXY(C) – SCHOTT NEXTERION E RINSED WITH ETOH PRIOR TO PRINTING, ITO – INDIUM TIN OXIDE COATED GLASS COVERSLIPS, NHS – SCHOTT NEXTERION H, PIRANHA – GLASS COVERSLIPS CLEANED IN PIRANHA SOLUTION, PLASMA GLASS COVERSLIPS CLEANED WITH OXYGEN PLASMA).

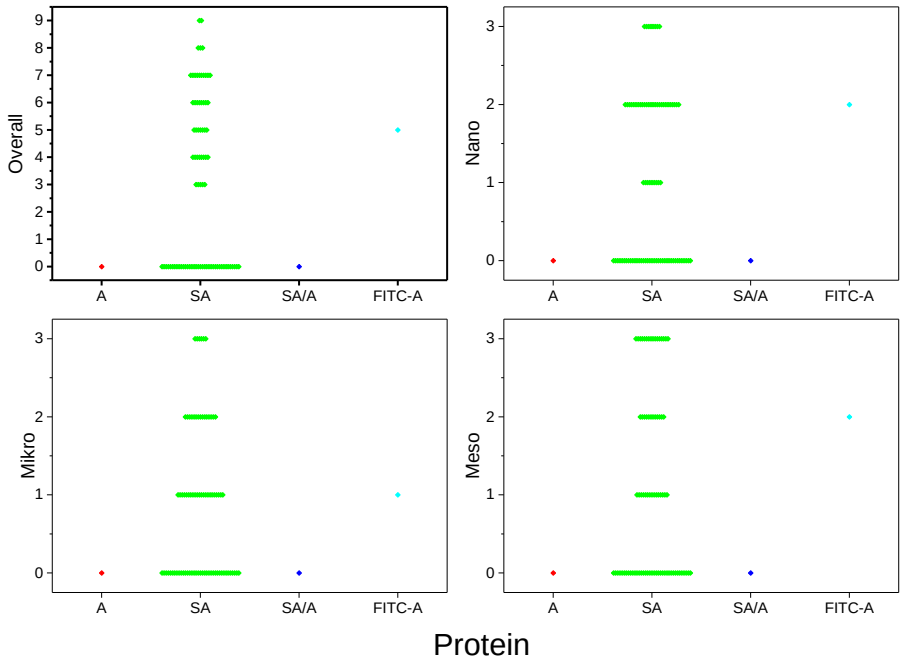

FIGURE 17: QUALITY OF IMPRINTS FOR DIFFERENT CHOICES OF DEPOSITED PROTEIN (A – AVIDIN, FITC-A – AVIDIN LABELLED WITH FLUOROPHORE FITC, SA – STREPTAVIDIN, SA/A MIXTURE OF STREPTAVIDIN AND AVIDIN).

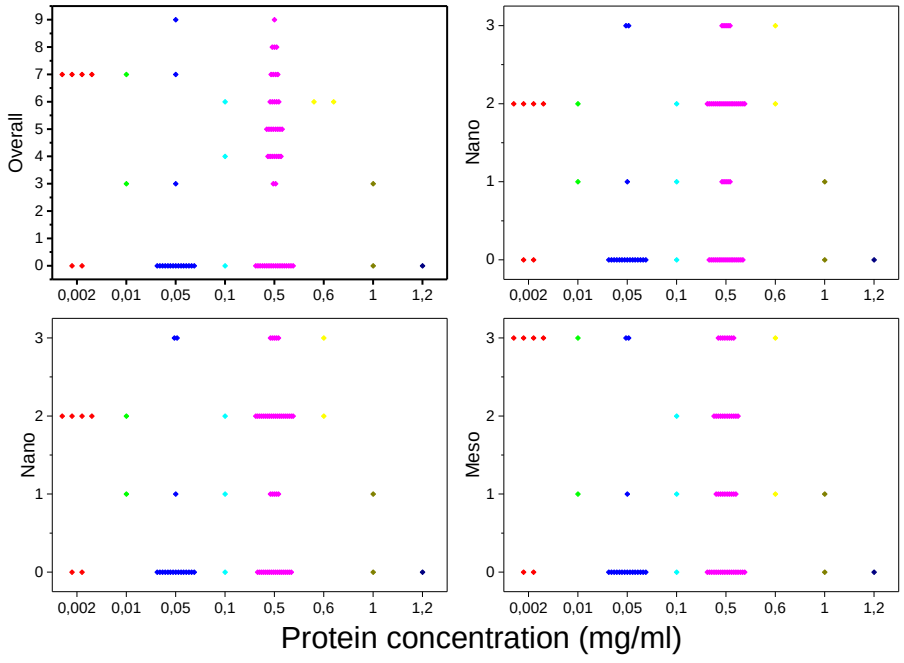

FIGURE 18: QUALITY OF IMPRINTS FOR DIFFERENT PROTEIN CONCENTRATION IN THE SOLUTION THAT IS INCUBATED ON THE POSS-STAMPS.

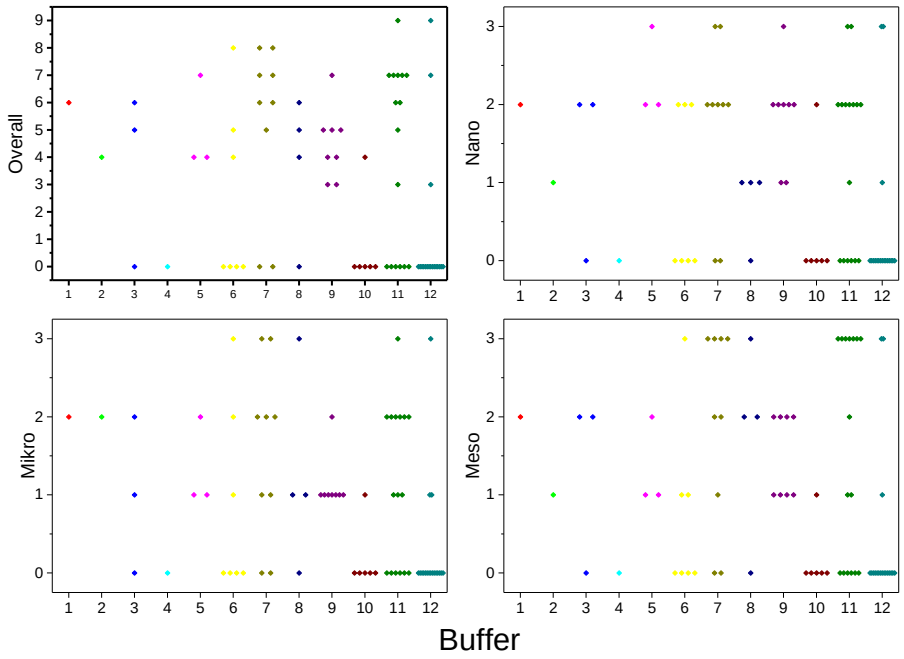

FIGURE 19: QUALITY OF IMPRINTS FOR A VARIETY OF BUFFERS. THE COMPOSITION OF THE BUFFERS HAS NOT BEEN PUBLISHED YET.

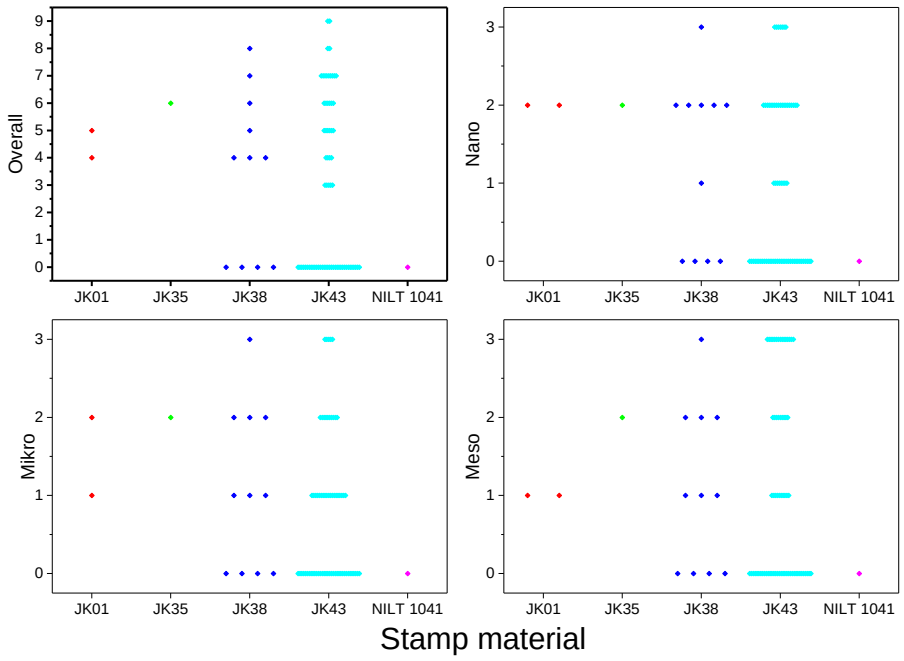

FIGURE 20: QUALITY OF IMPRINTS FOR DIFFERENT POSS COMPOSITIONS. (JK01 – 8 EPOXY-HEXENE; JK35 – 4 EPOXY-HEXENE, 4 METHYLALLYLACETIC ACID; JK38 4 EPOXY-HEXENE, 4 ALLYLACETIC ACID; JK43 5 EPOXY-HEXENE, 3 METHYLALLYLACETIC ACID)

4.2 PRINTING PROTOCOL

From the beginning of the project it was clear that the imprint protocol developed for PDMS stamps could serve as a blueprint also for stamps from materials more suitable for nanoscale lithography, but that major alterations to the protocol were needed to take the different material properties into account.

Stamping with PDMS is usually done by careful manual manipulation as the stamp itself adheres to the glass. This does not hold true for POSS. Our partners at Profactor use an EVG 620 wafer alignment tool to mount the stamp, align it to the substrate and apply defined pressure.

4.2.1 STAMP REUSE

The current stamp layout is a 4-inch silicon wafer with 230 nm lines at the whole wafer. The wafer can be broken and shards can be used as stamps. The goal of the project is to transfer the knowledge gained from this layout to stamps with smaller linewidths. Their layout is more lavish: one wafer only hosts one stamp, and therefore it would be efficient to be able to use stamps multiple times (Figure 23).

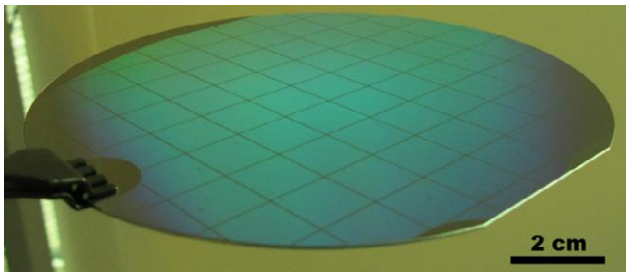

FIGURE 21: 4'' SI-WAFER WITH POSS STRUCTURE (230 NM LINES, 500 NM PERIOD), (KASTNER ET AL., 2014).

4.2.2 INCUBATION TIME

To get a layer of protein a drop of buffer solution containing the protein is placed on the stamp. After this incubation time the drop is removed by either blow drying in a nitrogen stream or spincoating. Residual salt is removed by rinsing with water followed again with blow drying or spincoating.

Here the different surface structures of POSS and PDMS largely influence the incubation time needed for a successful imprint. PDMS has a rather spongy appearance. Protein and solvent can diffuse into the stamp, which increases the effective surface area. The PDMS protocol therefore recommends no less than 15 minutes to saturate the upper layers of the stamp. We showed that far smaller incubation time is sufficient for POSS materials (Figure 24).

4.2.3 *Print duration*

The protocol for PDMS stamps schedules stamps-glass substrate contact times of at least one hour at room temperature or overnight in the fridge at 4° C. Due to the above mentioned bulkier properties of POSS Streptavidin should be available immediately at the interface and therefore less imprint time is needed (Figure 25).

4.2.4 *Stamp mount*

At the beginning of the project the stamp machine was not used in the way it was intended to be used. Instead of mounting the stamp to the chuck the stamp was put loosely on the glass substrate and then just pressed (Figure 22, left). The reason for that was that the stamp size was not large enough to cover the vacuum mechanism that should grab the stamp. Later, a different technique, which improved the alignment (Figure 26), was used. The stamp was glued to a piece of PDMS and then to a microscope slide that is large enough to cover the air outlets (Figure 22, right). As glue material Ormostamp, a popular resist in the lithography industry, and instant adhesive were used.

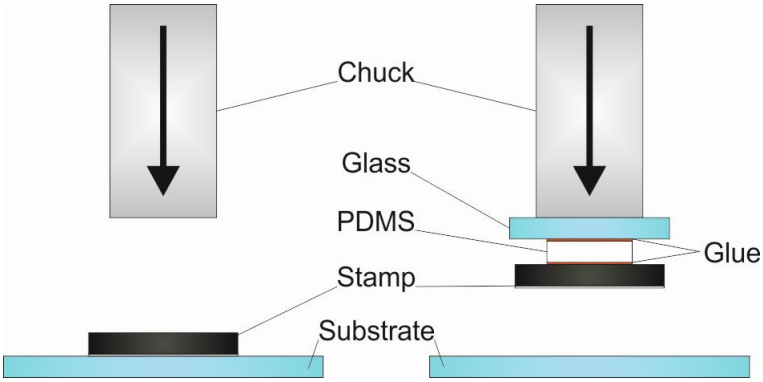

Figure 22: For the imprint the stamp was either loosely placed on the glass substrate and then pressed or mounted as a stamp-PDMS-glass composite on the chuck. Ormostamp and instant adhesive were tested as glue materials.

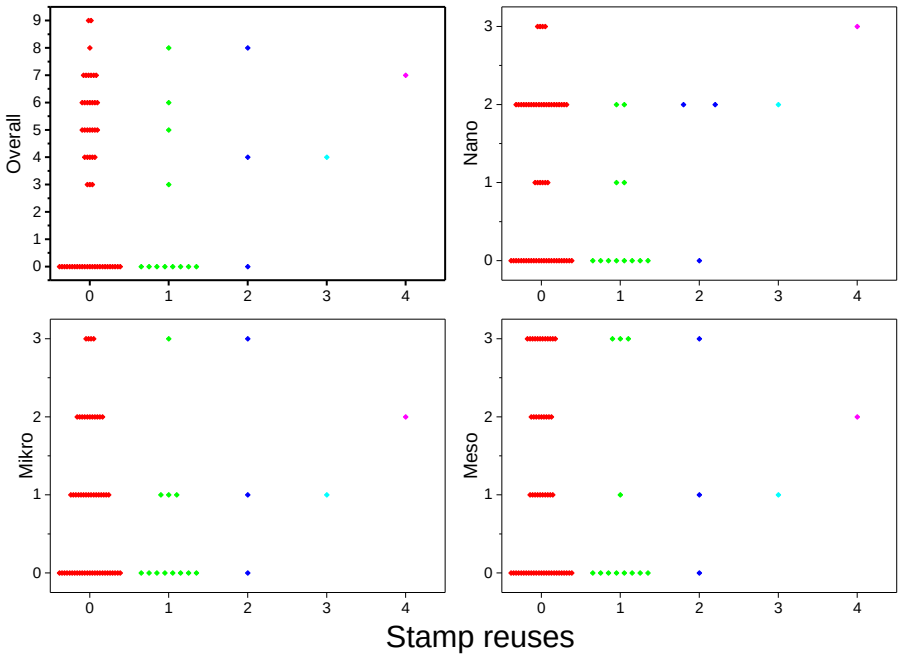

FIGURE 23: QUALITY OF IMPRINTS DEPENDENT ON THE NUMBER OF TIMES THE STAMP HAS BEEN REUSED.

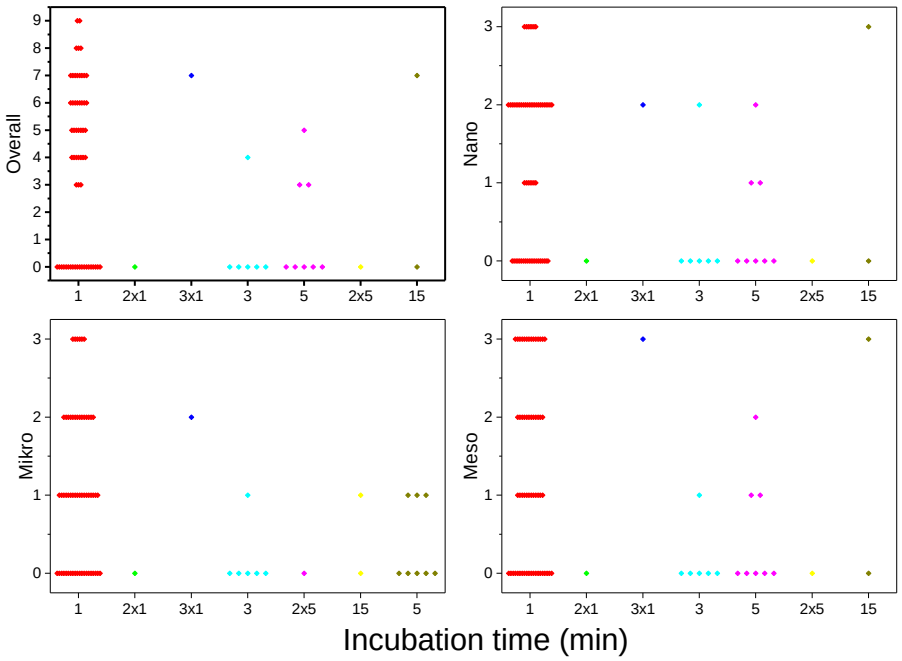

FIGURE 24: QUALITY OF IMPRINTS DEPENDENT ON THE TIME THE PROTEIN SOLUTION WAS INCUBATED ON THE STAMP BEFORE THE IMPRINT PROCESS.

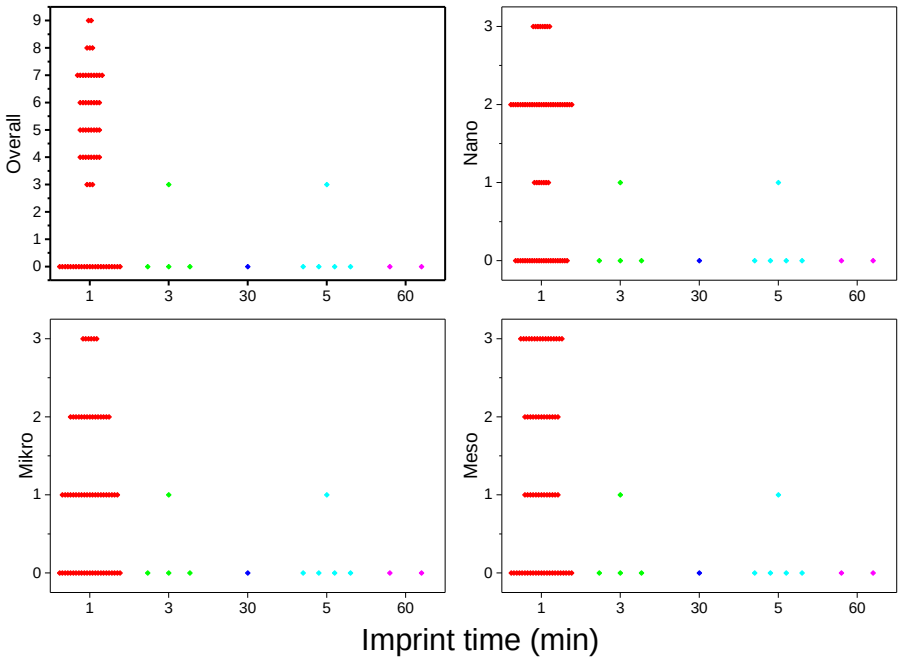

FIGURE 25: QUALITY OF IMPRINTS DEPENDENT ON THE TIME THE STAMP WAS PRESSED ONTO THE GLASS SUBSTRATE DURING THE IMPRINT PROCESS.

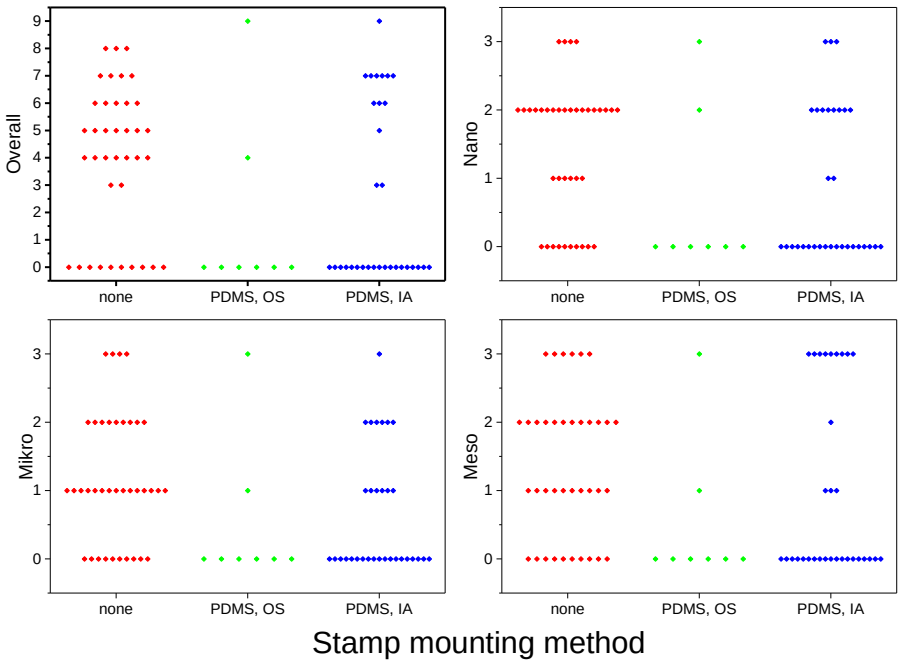

FIGURE 26: QUALITY OF IMPRINTS FOR DIFFERENT POSSIBILITIES OF MOUNTING THE STAMP ON THE IMPRINT MACHINE. THE STAMP WAS EITHER JUST LOOSELY PLACED ON THE GLASS SUBSTRATE (NONE) OR MOUNTED VIA A

STAMP-PDMS-SLIDE-COMPOSITE GLUED TOGETHER WITH ORMOSTAMP (PDMS, OS) OR INSTANT ADHESIVE (PDMS, IA).

4.3 POST-TREATMENT

It could have been possible that the protein was transferred to the glass substrate, but successful covalent binding did not happen and Streptavidin was then lost during transport or upon contact with liquid. The imprint machine does not allow for varying environmental parameters during the imprint, but the slides could be exposed to different atmospheres immediately after.

For shipment and storing the samples have to be dried. Streptavidin is a robust protein, but it might be affected by inhospitable conditions. When residual water evaporates from the imprinted glass protein and salt concentration rise and acidity might change. This could happen very localized so that on one slide many different conditions may be present.

These preferable or undesirable local chemical environments could explain why occasionally lines could only be found in the vicinity of contaminations on the surface (Figure 27). Such pollutions could have acted as anchors for a receding liquid film.

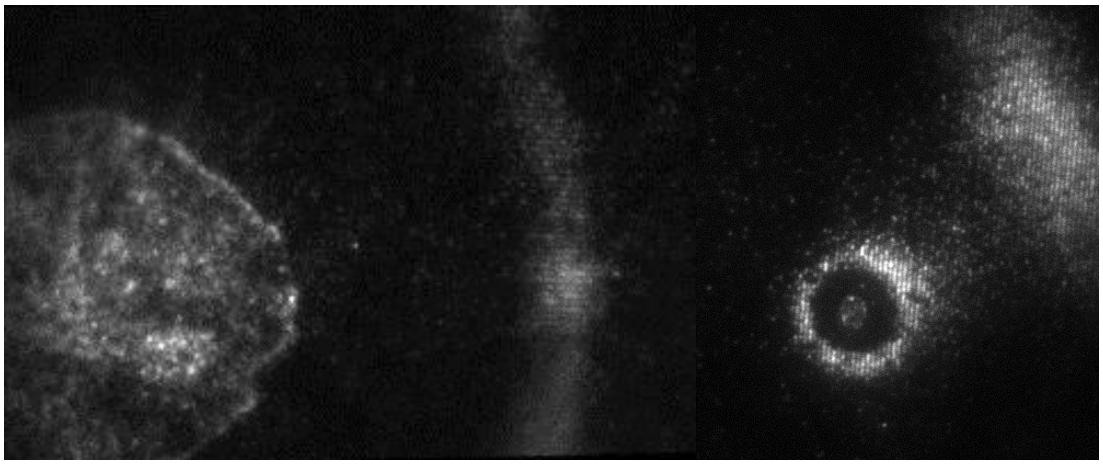

FIGURE 27: ON VERY LOW QUALITY IMPRINTS LINES CAN OCCASIONALLY BE FOUND SURROUNDING CONTAMINATIONS.

4.3.1 HUMIDITY

Streptavidin presumably binds to the functionalized glass substrate only in the presence of buffer. If a thin liquid film remains after the imprint, the exposure to air will dry it out and no reactions between the protein and the glass slide will take place any more. By putting the sample in a closed chamber, which contains a reservoir of water, the ambient humidity can be increased and the drying rate could be slowed down, thereby prolonging the time in which Streptavidin could bind to the functional groups on the surface (Figure 28).

4.3.2 TEMPERATURE

A possible parameter to control binding kinetics is temperature. According to the Arrhenius equation the binding rate increases with temperature. To test a dependence the sample after the imprint was either allowed to rest at room temperature (22°C) or was placed in the fridge (4°C) or in an incubator (40°C or 50°C) (Figure 29).

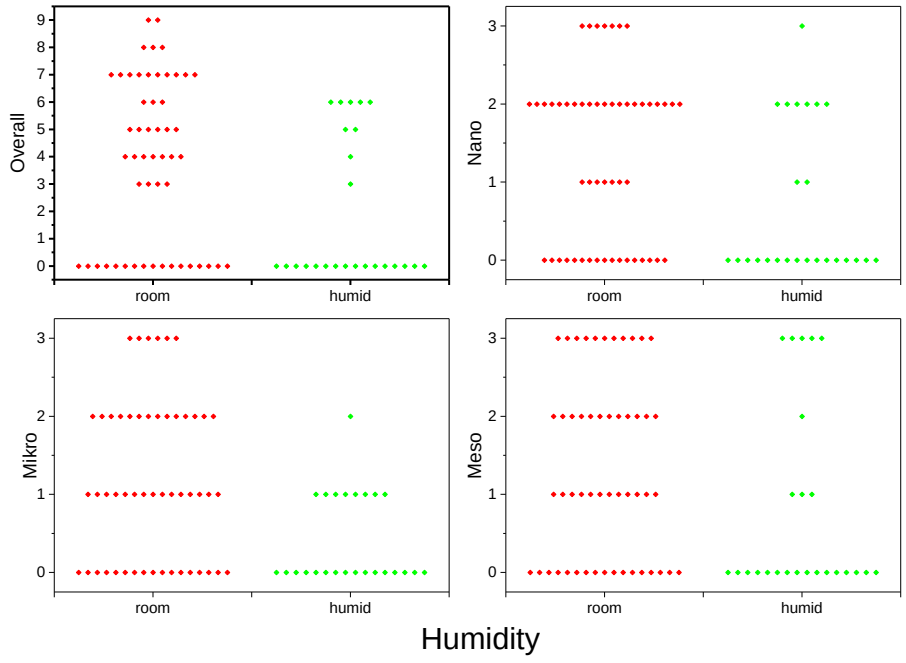

FIGURE 28: QUALITY OF IMPRINTS FOR DIFFERENT ENVIRONMENTS AFTER THE IMPRINT PROCESS. SAMPLES WERE EITHER STORED IN A HUMIDITY CHAMBER OR AT ROOM CONDITIONS.

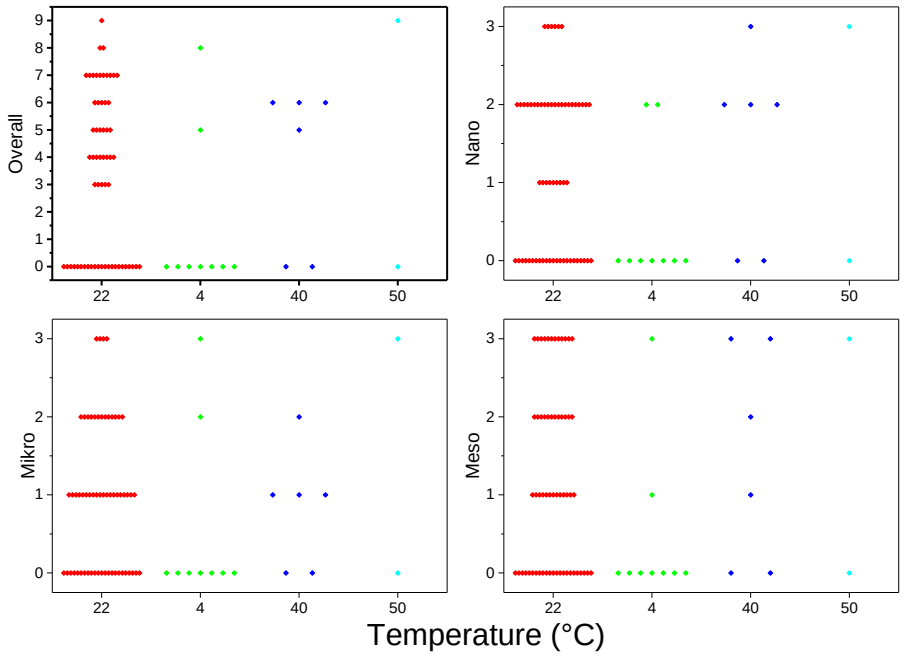

FIGURE 29: QUALITY OF IMPRINTS FOR DIFFERENT ENVIRONMENTS AFTER THE IMPRINT PROCESS. SAMPLES WERE EITHER STORED IN A FRIDGE, AT ROOM CONDITIONS OR IN A HEAT CHAMBER.

4.4 TRANSPORT AND STORING

4.4.1 TRANSPORT

The samples were printed in the clean room lab at Profactor in Steyr and shipped overnight via mail to the Vienna University of Technology. The conditions during the transport could only be supervised in a few occasions where they were transported by members of the team.

The package usually was sealed airtight; a parameter that could have influenced the quality of the structures could have been temperature during transport. Temperature was not monitored; an influence should be reflected in differing results for deliveries during for cold and warm months (Figure 30).

4.4.2 STORAGE TIME

Not all samples could be imaged within short time after arrival potential, so until they were characterized they were stored in the fridge. We tested whether degrading of glass substrate

or Streptavidin with time might have affected line quality (Figure 31). Failed imprints were excluded from the analysis as they are considered not to be caused by long storage but by faulty imprints.

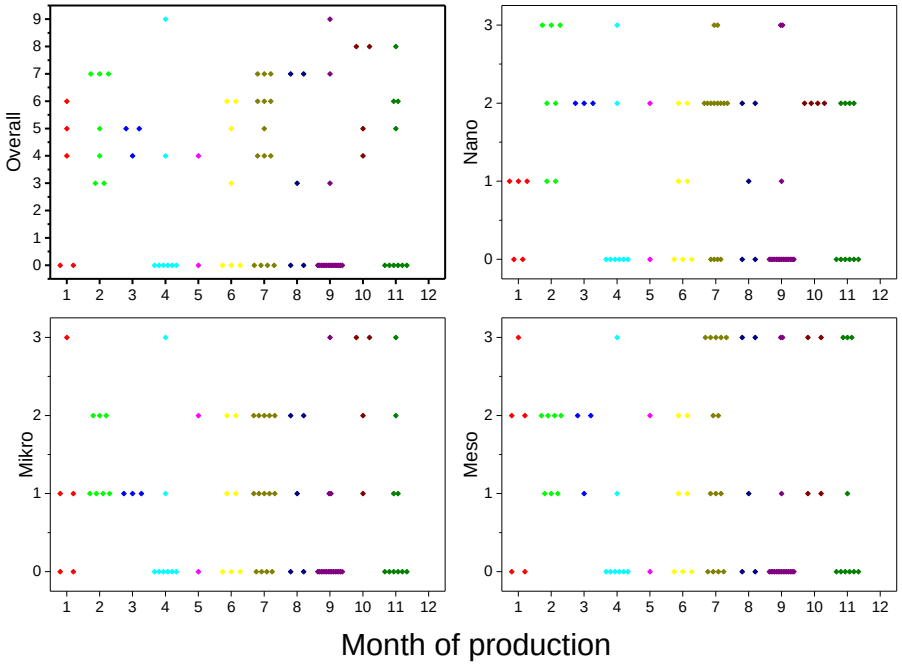

FIGURE 30: QUALITY OF IMPRINTS DEPENDENT ON THE MONTH OF PRODUCTION.

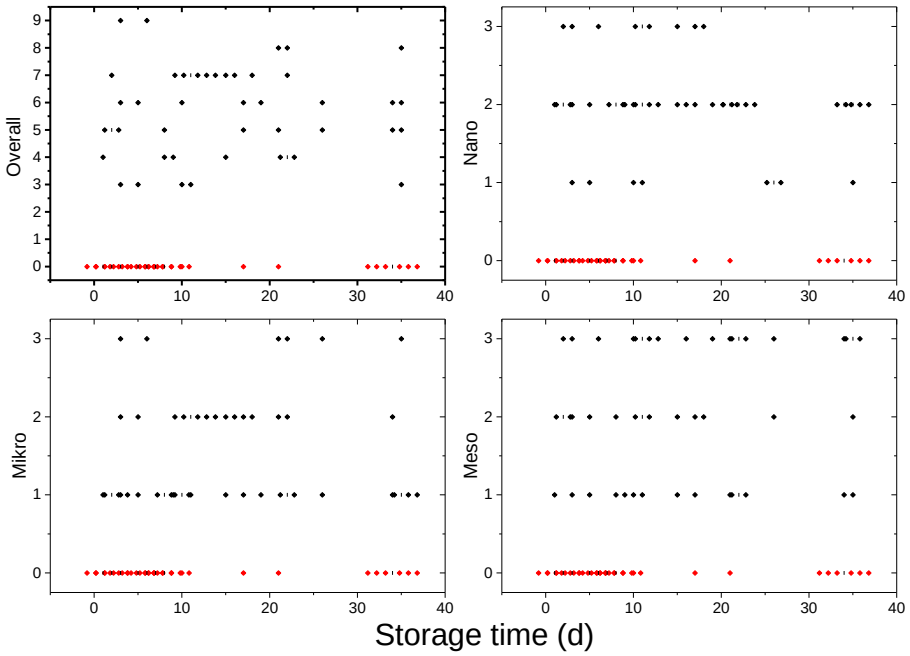

FIGURE 31: QUALITY OF IMPRINTS AS A FUNCTION OF TIME PASSED BETWEEN MANUFACTURING AND MEASUREMENT.

4.5 NANOSCALE CHARACTERIZATION WITH DSTORM AND AFM

We used dSTORM to gain insights into the nanoscale organization of streptavidin molecules within the structures, which helps in developing models how deposition works and why imprints may have failed.

To search for interesting areas we used conventional fluorescence microscopy with low illumination power so that the fluorophores were bleached as little as possible. In order to increase the image acquisition rate we did not read out the whole EM-CCD chip, but cropped the image so that squares with a side length of 7 or 14 µm were imaged.

The Alexa 647N fluorophore that we used exhibits suitable switching characteristics for dSTORM if the buffer on the sample is exchanged with ROXS buffer. Recording 5000 -10000 frames is easily achievable. As the ROXS buffer minimizes photobleaching often even a second imaging cycle on a previously illuminated spot can be done.

It is important that an imaged flourophore enters the triplet state after imaging. The probability for the transition scales with the number of times the molecule enters the excited state. We control this by increasing or decreasing the illumination time. Also varying illumination intensity would allow this, but for dSTORM measurements the laser was already operated at maximum power, therefore upregulation was not possible.

The reconstruction of the image from the recorded stack was done with rapidSTORM 3.2 (Wolter et al., 2012).

The superresolution images show that functional Streptavidin does not homogenously coat the glass surface. The structures consist of clusters with an approximate signal FWHM of 50 to 100 nm.

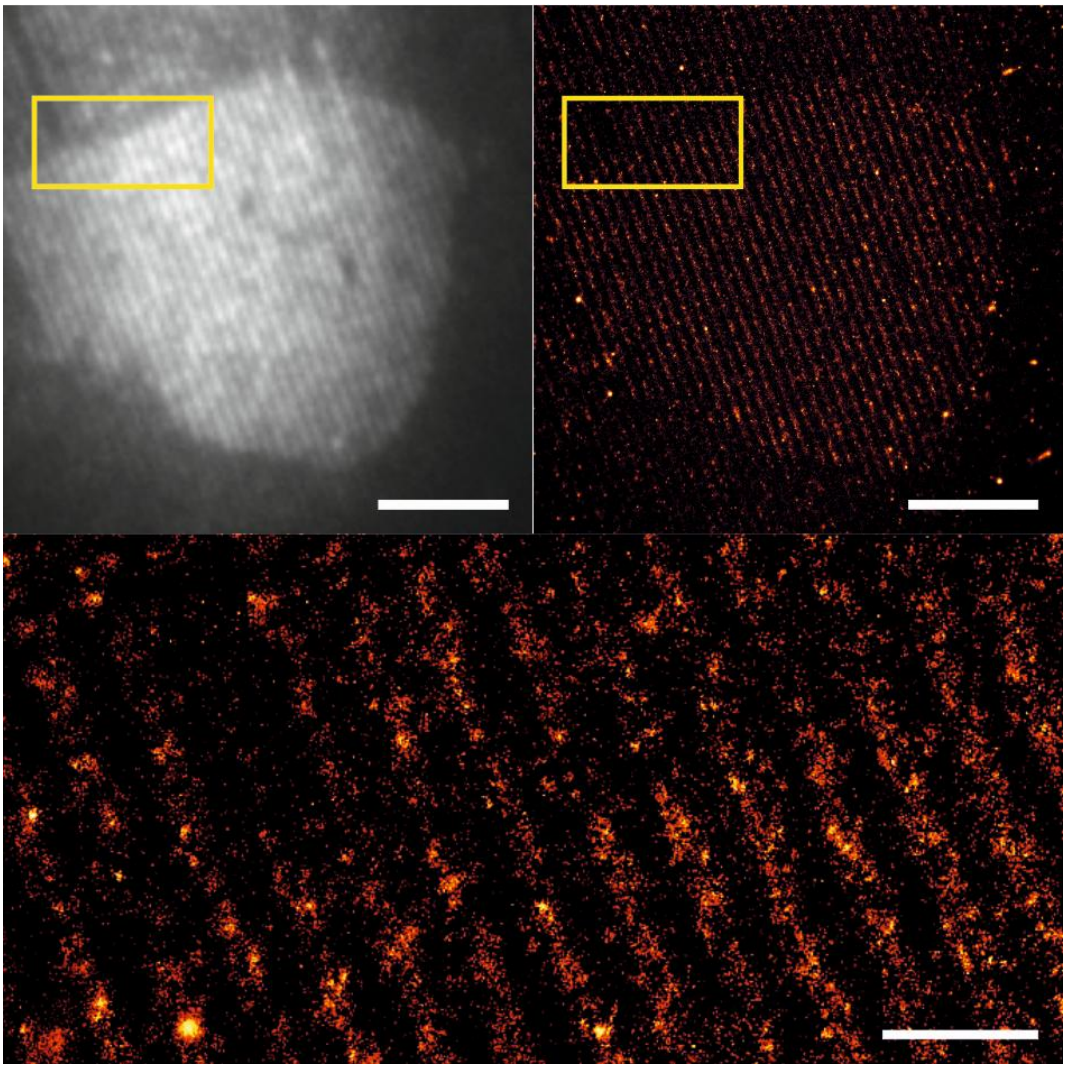

FIGURE 32: COMPARISON OF CONVENTIONAL FLUORESCENCE (TOP LEFT) AND DSTORM (TOP RIGHT) IMAGES. MAGNIFICATION OF SECTION OF DSTORM IMAGE IN BOX (BOTTOM). SCALE BARS 5 µM TOP ROW, 1 µM BOTTOM.

AFM experiments were performed in contact mode using the JPK NanoWizard 3 with NanoWorld CONTR cantilevers. The pixel size was chosen to approximately fit the nominal tip curvature radius of 10 nm. We tried to use as little force as possible to probe the sample, otherwise the shear forces would have been sufficient to remove the structures from the glass substrate. Typical line rates used for imaging were 0.5 to 2 Hz.

Imaging was done both in air and in liquid after the incubation of the antibody. The latter proved to be more difficult as BSA has similar height as the antibodies on Streptavidin (Figure 33).

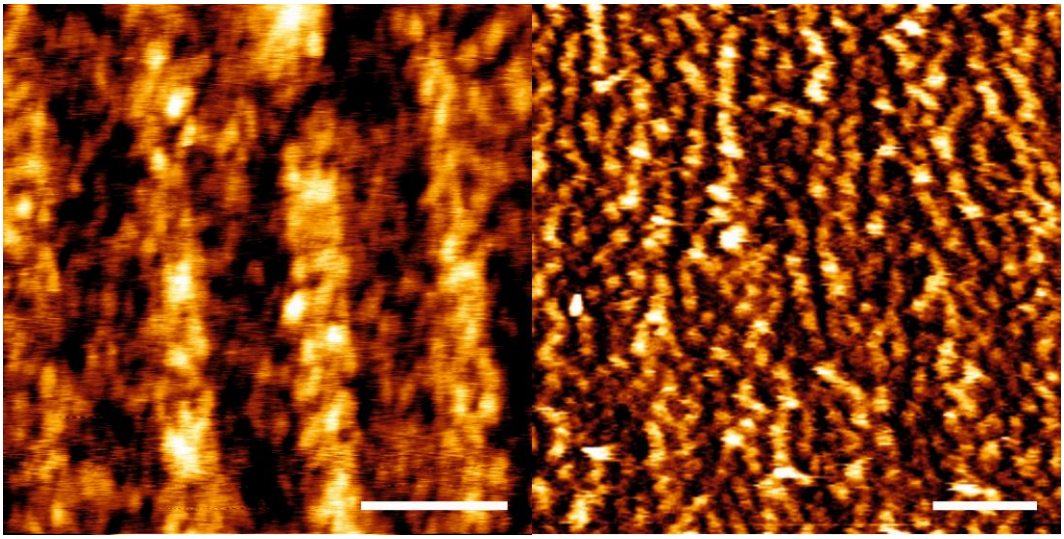

FIGURE 33: COMPARISON OF AFM IMAGES IN AIR (LEFT) AND IN PBS BUFFER (RIGHT). THE AIR IMAGE SHOWS DEPOSITED STREPTAVIDIN ON EPOXY GLASS SUBSTRATE. THE SAMPLE ON THE RIGHT SIDE IS THE SAME IMPRINT AFTER INCUBATION OF ANTIBODY AND BSA. SCALE BAR 500NM.

AFM images in air (Figure 34support the theory of streptavidin being deposited in lumps, as distinct clusters can also be seen.

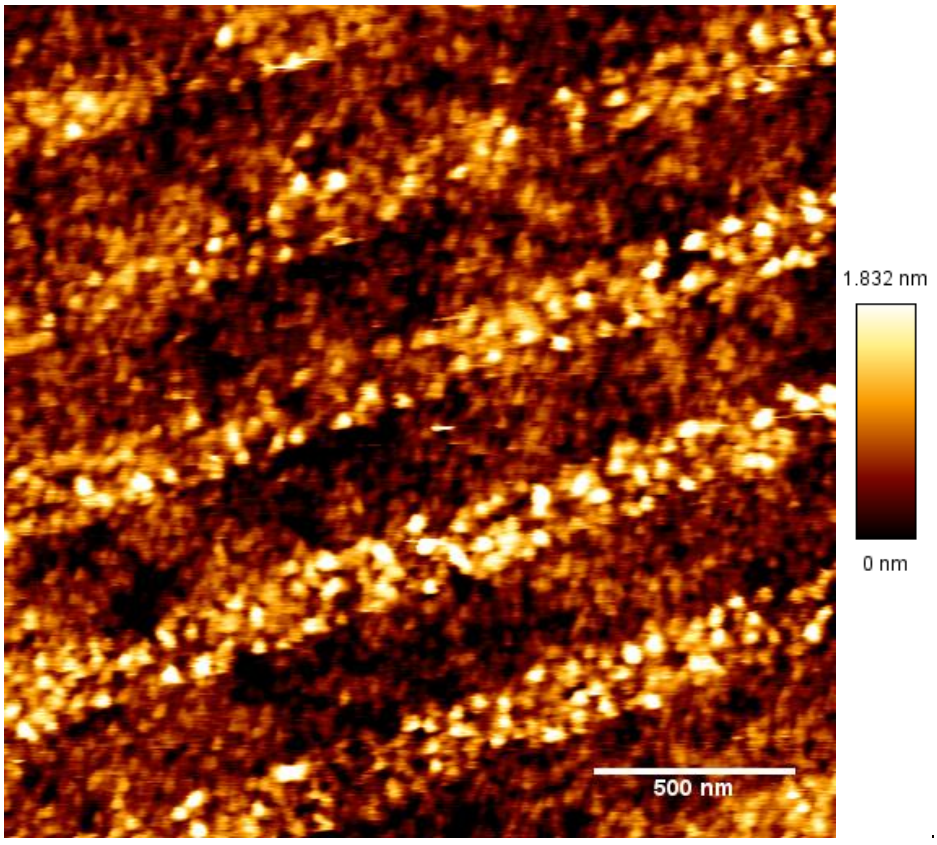

FIGURE 34: AFM IMAGES OF DEPOSITED STREPTAVIDIN IN AIR.

4.6 LIVE CELLS INTERACTING WITH STRUCTURES

The original task of testing live cells on nanopatterns was delayed due to the prolonged search for suitable parameters for the manufacturing of those patterns.

Jurkat cells were cultured in fully supplemented RPMI medium at 37°C and 5% CO2. For measurements 1-5 ml (depending on the density of cells) were taken from the cell suspension and centrifuged at 1000 rpm to pelletize the cells and remove the supernatant growing medium.RPMI contains fluorescent ingredients, so it were replaced by 0.5-1 ml of Hank's Buffered Salt Solution (HBSS). Meanwhile the coverslips that were incubated with anti-CD4 antibody had been warmed up to 37°C. Cells were allowed to settle 5-10 minutes at 37°C before the measurement.
Cell imaging was done at room temperature.

RICM images (see Figure 35) show that filopodia seem to align with the given nanopatterns, which is not surprising as the inert BSA between the lines of antibodies prevents adhesion. Directionality of the cell body however could not be seen so far.

The cells attached firmly to the substrate. Whether the granular structure of the cell body (Figure 35) is caused by reflections of organelles close to the membrane or plasma membrane ruffles still has to be determined. Direct dependence on the line structure – colocalization – cannot be measured. This indicates that the lines seen in fluorescence measurements (Figure 36) originate from protein reorganization and not from topology effects.

So far only a limited number of PALM experiments could be performed. Although the contrast of the image is not optimal lines in the plasma membrane are recognizable (Figure 37).

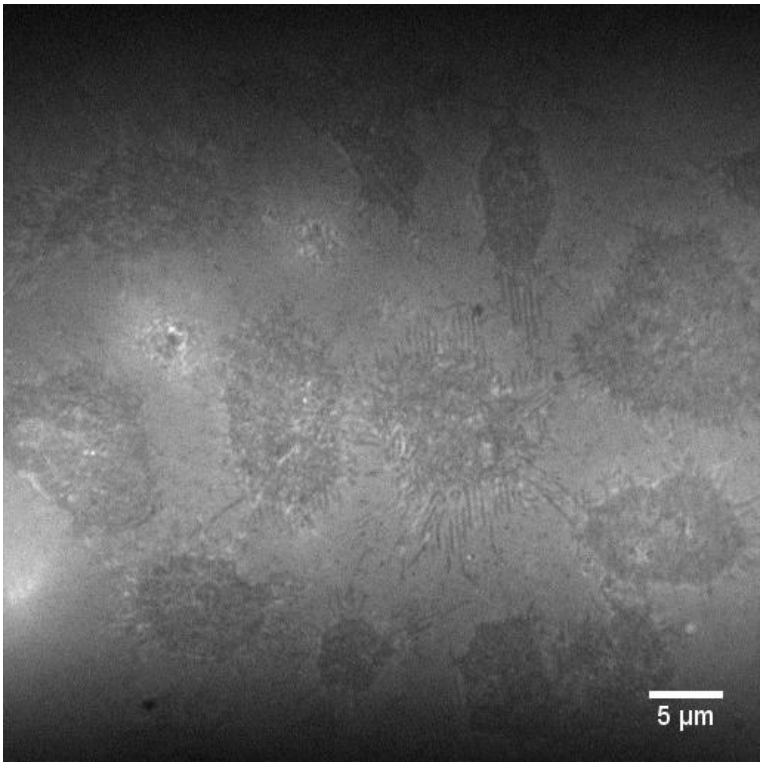

FIGURE 35: IRM IMAGE OF JCAM 1.6 CELLS TRANSFECTED WITH CD4 AND HLCK-MEOS3.2 ON ANTI-CD4 NANOPATTERN. CELL FILOPODIA ALIGN THEMSELVES ALONG THE PATTERN.

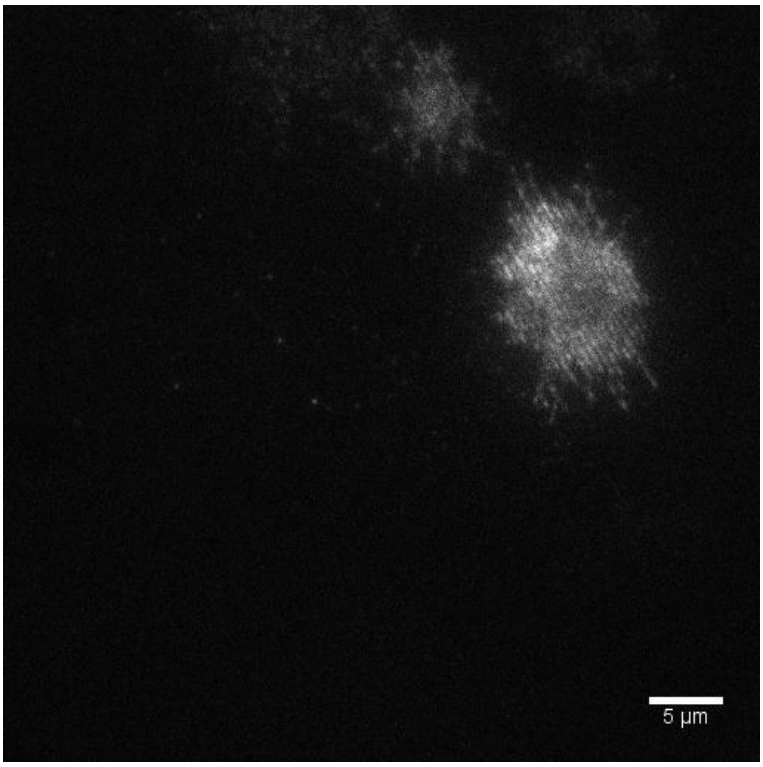

FIGURE 36: FLUORESCENCE MICROSCOPY IMAGE OF JCAM 1.6 CELLS TRANSFECTED WITH CD4 AND HLCK-MEOS3.2 ON ANTI-CD4 NANOPATTERN.

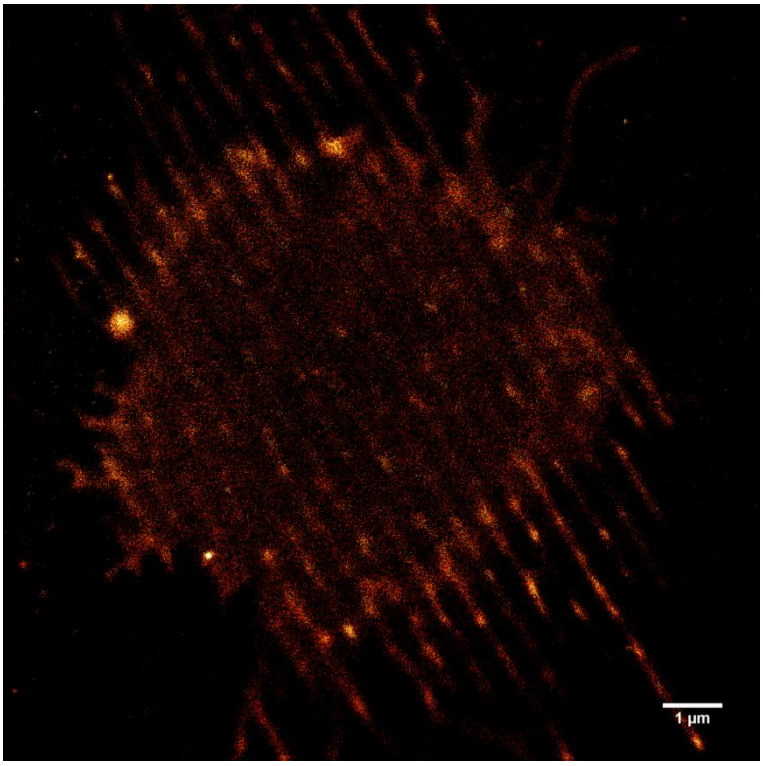

FIGURE 37: PALM IMAGE OF JCAM 1.6 CELLS TRANSFECTED WITH CD4 AND HLCK-MEOS3.2 ON ANTI-CD4 NANOPATTERN.

5 INTERPRETATION OF RESULTS, CONCLUSION AND OUTLOOK

Materials:

Schott functionalized coverslips delivered a wide range of outcomes. Tests with aldehyde and NHS-ester containing surface chemistries showed no advantages over the cheaper epoxy-based surface covering (Figure 16). A higher reactivity of epoxy slides after $EtOH$ treatment as suggested by the protocol for PDMS stamps could not be found.

Functionalized glass slides can be a source of error. They underwent quality control at the vendor, but to us it was not known whether coatings from different batches can be considered equally suitable for our purpose and whether clustering of deposited protein could be linked to nanoscale inhomogeneities of the substrate.

The low success rate might indicate that in spite of the functionalization covalent bond formation did not always occur; in fact, protein coating may have relied on other interactions, which could alternatively be provided by simple and more economic surface treatments. For

example, experiments with plasma cleaned slides resulted in fair quality (Figure 16). A late experiment with piranha solution treated glass showed potential (Figure 14, top right). Further experiments are required to assess the suitability of this method for live cell experiments. ITO slides failed all requirements as Streptavidin denatured on this surface.

The nominal concentration of Streptavidin in the solution that is incubated on the stamp does not influence the quality of imprints within the range that was covered in the thesis (Figure 18). Even for concentrations as small as 0.002 mg/ml enough protein was provided to facilitate successful printing.

From the variety of buffers that were used, none provided exceptional results (Figure 19). We noticed a slightly worse performance with acidic buffers.

The two most used stamp material – JK38 and JK43 - produced similar results (Figure 19). AFM force spectroscopy experiments at Profactor did not reveal conclusive proof whether the initial idea of functional groups at the surface of the stamps providing electrostatic affinity for Streptavidin holds true. It is not clear whether those groups are accessible at the surface or incorporated in the bulk.

The storage time of the materials was not recorded; therefore aging effects on the quality of the imprints could not be examined. For Streptavidin, buffer and glass slides one can assume a period of utilization of around 6 months. The time period from production to usage of stamps was distinctly longer.

Printing protocol:

Only a rather small amount of data on the reusability of stamps could be obtained so far, significant decrease in imprint quality with multiple uses of stamps was not observed therein (Figure 23). However our partners from Profactor observed the deposition of unknown material on the stamps. The nature of this plaque, its removal and the influence of cleaning procedures will be the subject of further study.

As far as incubation (Figure 24) and imprint (Figure 25) are concerned timing does not seem to be critical.

An advantage of proper mounting of the stamp can be seen in better meso scale homogeneity (Figure 26). Planar alignment and guided movement of the stamp during the printing process leads to a larger area of usable lines for cell experiments.

The printing protocol contains uncertainties. Especially the stamp handling procedure prior to the imprinting is difficult to quantify. It includes a washing step to remove excess materials of Streptavidin, leaving only a monolayer on the surface of the stamp. Rinsing with deionized

water should remove excess of PBS to prevent the formation of salt crystals during the following drying. Several scenarios can be imagined why this is the critical step for successful imprinting. In conjunction with the unknown functional groups on the surface of the stamp the unnatural condition of salt-less solute could lead to denaturation of the protein. After washing the stamp is spin-coated to remove the excess of water, presumably leaving only a thin film of water to provide an aqueous environment, in which the covalent binding of Streptavidin to the glass substrate should happen. It is plausible that the amount of water at the stamp-glass interface largely depends on atmospheric conditions in the room or the time needed to manipulate stamp and glass. If not enough water is on the stamp the protein solution might dry out. This could explain the high rate of failed imprints. This issue is less critical when using PDMS stamps because their spongy morphology provides a reservoir of water. As this effect would be very sensitive to time, finding appropriate measurement techniques will be challenging.

Post-treatment:

Neither humidity (Figure 28) nor temperature (Figure 29) after the imprint seem to influence the quality of the pattern. This could be seen as an indication that all buffer is depleted within a very short time after a successful imprint and Streptavidin and glass surface have little time to form covalent bonds.

Transport and storage

In general imprints seem to maintain their quality on the long term. We could not find evidence for seasonal dependence and concomitantly hot or cold temperatures during the transport (Figure 30). Also we could not record a significant influence of storing in the fridge for times below 40 days (Figure 31).

Nanostructure:

Both AFM and optical superresolution imaging reveal that the lines exhibit an underlying substructure of distinct clusters. It is yet unclear how these structures form. On the one hand, the reactive groups on the substrates could induce conformational changes on the proteins, thereby enhancing the clustering tendency. On the other hand, also the drying process could have similar effects. Nanoscale inhomogeneities of the stamp can also effect clustering of proteins, however, our partners could not find irregularities in the stamp topology.

Live cell experiments:

We could show that if both cells and suitable structures are available experiments initially done on microstructures can be performed using the new nanostructures.. Smaller inter-structure

distances might even provide more reliable results as membrane buckling and liquid accumulation under the membrane can easier be avoided due to the more dispersed anchoring.

REFERENCES

Axelrod, D. (1989). Total internal reflection fluorescence microscopy. *Methods Cell Biol, 30*, 245-270.

Barr, V. A., & Bunnell, S. C. (2009). Interference reflection microscopy. *Curr Protoc Cell Biol, Chapter 4*, Unit 4 23. doi: 10.1002/0471143030.cb0423s45

Beaumont, P. C., Johnson, D. G., & Parsons, B. J. (1997). Excited state and free radical properties of rhodamine dyes in aqueous solution: A laser flash photolysis and pulse radiolysis study. *Journal of Photochemistry and Photobiology A: Chemistry, 107*(1), 175-183.

Beck, K., & Bereiter-Hahn, J. (1981). Evaluation of Reflection Interference Contrast Microscope Images of Living Cells. *Microscopica Acta, 84*(2), 153-178.

Bereiter-Hahn, J., Fox, C. H., & Thorell, B. (1979). Quantitative reflection contrast microscopy of living cells. *The Journal of Cell Biology, 82*(3), 767-779.

Berlier, J. E., Rothe, A., Buller, G., Bradford, J., Gray, D. R., Filanoski, B. J., . . . Haugland, R. P. (2003). Quantitative comparison of long-wavelength Alexa Fluor dyes to Cy dyes: fluorescence of the dyes and their bioconjugates. *J Histochem Cytochem, 51*(12), 1699-1712.

Betzig, E., Patterson, G. H., Sougrat, R., Lindwasser, O. W., Olenych, S., Bonifacino, J. S., . . . Hess, H. F. (2006). Imaging Intracellular Fluorescent Proteins at Nanometer Resolution. *Science, 313*, 1642-1645.

Binnig, G., & Rohrer, H. (1986). Scanning Tunneling Microscopy. *Ibm Journal of Research and Development, 30*(4), 355-369.

Born, M., & Wolf, E. (1999). *Principles of Optics*. Cambridge, UK: Cambridge University Press.

Bubenik, J., Barešová, M., Viklický, V., Jakoubkova, J., Sainerova, H., & Donner, J. (1973). Established cell line of urinary bladder carcinoma (T24) containing tumour-specific antigen. *International Journal of Cancer, 11*(3), 765-773.

Bückers, J., Wildanger, D., Vicidomini, G., Kastrup, L., & Hell, S. W. (2011). Simultaneous multi-lifetime multi-color STED imaging for colocalization analyses. *Optics Express, 19*(4), 3130-3143. doi: 10.1364/OE.19.003130

Eigen, M., & Rigler, R. (1994). Sorting single molecules: application to diagnostics and evolutionary biotechnology. *Proc Natl Acad Sci U S A, 91*(13), 5740-5747.

Fernandez-Suarez, M., & Ting, A. Y. (2008). Fluorescent probes for super-resolution imaging in living cells. *Nat Rev Mol Cell Biol, 9*(12), 929-943. doi: 10.1038/nrm2531

Heilemann, M., van de Linde, S., Schuttpelz, M., Kasper, R., Seefeldt, B., Mukherjee, A., . . . Sauer, M. (2008). Subdiffraction-resolution fluorescence imaging with conventional fluorescent probes. *Angew Chem Int Ed Engl, 47*(33), 6172-6176. doi: 10.1002/anie.200802376

Hell, S. W. (2007). Far-field optical nanoscopy. *Science, 316*(5828), 1153-1158.

Hell, S. W., & Wichmann, J. (1994). Breaking the diffraction resolution limit by stimulated emission: stimulated-emission-depletion fluorescence microscopy. *Opt Lett, 19*(11), 780-782.

Hess, S. T., Girirajan, T. P., & Mason, M. D. (2006). Ultra-high resolution imaging by fluorescence photoactivation localization microscopy. *Biophys J, 91*(11), 4258-4272.

Hutter, J. L., & Bechhoefer, J. (1993). Calibration of Atomic-Force Microscope Tips. *Review of Scientific Instruments, 64*(7), 1868-1873. doi: Doi 10.1063/1.1143970

Izzard, C. S., & Lochner, L. R. (1976). Cell-to-substrate contacts in living fibroblasts: an interference reflexion study with an evaluation of the technique. *J Cell Sci, 21*(1), 129-159.

Jaiswal, J. K., & Simon, S. M. (2004). Potentials and pitfalls of fluorescent quantum dots for biological imaging. *Trends in Cell Biology, 14*(9), 497-504. doi: http://dx.doi.org/10.1016/j.tcb.2004.07.012

Kastner, J., Lorret, O., Rank, A., Schwarzinger, C., Dittert, B., & Mühlberger, M. (2014). Nanocontact Printing Stamp Material via Bi-functionalization of Polyhedral Oligomeric Silsesquioxanes. *European Polymer Journal*. doi: 10.1016/j.eurpolymj.2014.11.015

Kuhn, B., Fromherz, P., & Denk, W. (2004). High sensitivity of Stark-shift voltage-sensing dyes by one- or two-photon excitation near the red spectral edge. *Biophys J, 87*(1), 631-639. doi: 10.1529/biophysj.104.040477

Patterson, G., Davidson, M., Manley, S., & Lippincott-Schwartz, J. (2010). Superresolution imaging using single-molecule localization. *Annu Rev Phys Chem, 61*, 345-367. doi: 10.1146/annurev.physchem.012809.103444

Phizicky, E. M., & Fields, S. (1995). Protein-protein interactions: methods for detection and analysis. *Microbiological reviews, 59*(1), 94-123.

Ploem, J. (1975). Reflection-contrast microscopy as a tool for investigation of the attachment of living cells to a glass surface. *Mononuclear phagocytes in immunity, infection and pathology. Blackwell, Oxford*, 405-421.

Qin, D., Xia, Y., & Whitesides, G. M. (2010). Soft lithography for micro-and nanoscale patterning. *Nature Protocols, 5*(3), 491-502.

Ruprecht, V., Brameshuber, M., & Schütz, G. J. (2010). Two-color single molecule tracking combined with photobleaching for the detection of rare molecular interactions in fluid biomembranes. *Soft Matter, 6*(3), 568-581.

Rust, M., Bates, M., & Zhuang, X. (2006). Sub-diffraction-limit imaging by stochastic optical reconstruction microscopy (STORM). *Nat Methods, 3*(10), 793-795.

Sauer, M., Hofkens, J., & Enderlein, J. (2011). *Handbook of fluorescence spectroscopy and imaging : from single molecules to ensembles*. Weinheim: Wiley-VCH.

Schmidt, R., Wurm, C. A., Jakobs, S., Engelhardt, J., Egner, A., & Hell, S. W. (2008). Spherical nanosized focal spot unravels the interior of cells. *Nat Methods, 5*(6), 539-544. doi: 10.1038/nmeth.1214

Schneider, U., Schwenk, H. U., & Bornkamm, G. (1977). Characterization of Ebv-Genome Negative Null and T-Cell Lines Derived from Children with Acute Lymphoblastic Leukemia and Leukemic Transformed Non-Hodgkin Lymphoma. *International Journal of Cancer, 19*(5), 621-626. doi: DOI 10.1002/ijc.2910190505

Schwartz, O. (2004). Image competition. *Nat Rev Mol Cell Biol, 5*(3), 175-175.

Schwarzenbacher, M., Kaltenbrunner, M., Brameshuber, M., Hesch, C., Paster, W., Weghuber, J., . . . Schütz, G. J. (2008). Micropatterning for quantitative analysis of protein-protein interactions in living cells. *Nat Methods, 5*(12), 1053-1060.

Shaner, N. C., Lambert, G. G., Chammas, A., Ni, Y., Cranfill, P. J., Baird, M. A., . . . Wang, J. (2013). A bright monomeric green fluorescent protein derived from Branchiostoma lanceolatum. *Nat Methods, 10*(5), 407-409. doi: 10.1038/nmeth.2413

Shimomura, O. (1979). Structure of the chromophore of< i> Aequorea</i> green fluorescent protein. *Febs Letters, 104*(2), 220-222.

Shroff, H., Galbraith, C. G., Galbraith, J. A., & Betzig, E. (2008). Live-cell photoactivated localization microscopy of nanoscale adhesion dynamics. *Nat Methods, 5*(5), 417-423.

Stahelin, R. V. (2013). Surface plasmon resonance: a useful technique for cell biologists to characterize biomolecular interactions. *Molecular Biology of the Cell, 24*(7), 883-886.

Thompson, R. E., Larson, D. R., & Webb, W. W. (2002). Precise nanometer localization analysis for individual fluorescent probes. *Biophys J, 82*(5), 2775-2783.

Vang, T., Liu, W. H., Delacroix, L., Wu, S., Vasile, S., Dahl, R., . . . Tautz, L. (2012). LYP inhibits T-cell activation when dissociated from CSK. *Nat Chem Biol, 8*(5), 437-446. doi: http://www.nature.com/nchembio/journal/v8/n5/abs/nchembio.916.html#supplementary-information

Wikipedia, viewed 16 December 2014
IRM:
<http://en.wikipedia.org/wiki/File:IRM_Interference_Reflection_Microscopy.svg>
Airy disk / Rayleigh criterion:
<http://en.wikipedia.org/wiki/File:Airy_disk_spacing_near_Rayleigh_criterion.png>

Wolter, S., Loschberger, A., Holm, T., Aufmkolk, S., Dabauvalle, M. C., van de Linde, S., & Sauer, M. (2012). rapidSTORM: accurate, fast open-source software for localization microscopy. *Nat Methods, 9*(11), 1040-1041. doi: nmeth.2224 [pii]

Zhang, M., Chang, H., Zhang, Y., Yu, J., Wu, L., Ji, W., . . . Xu, T. (2012). Rational design of true monomeric and bright photoactivatable fluorescent proteins. *Nature Methods, 9*(7), 727-729. doi: 10.1038/nmeth.2021